Mathematical Modelling and Numerical Simulation of Marine Ecosystems With Applications to Ice Algae

by

Shyamila Iroshi Perera Wickramage

A thesis
presented to the University of Waterloo
in fulfillment of the
thesis requirement for the degree of
Master of Mathematics
in
Applied Mathematics

Waterloo, Ontario, Canada, 2013

I hereby declare that I am the sole author of this thesis. This is a true copy of the thesis, including any required final revisions, as accepted by my examiners.

I understand that my thesis may be made electronically available to the public.

Abstract

Sea-ice ecosystem modelling is a novel field of research. In this thesis, the main organism studied is sea-ice algae. A basic introduction to algae and its importance in the aquatic food web is given first. An introduction to modeling and its purposes is presented, and this is followed by a brief description of ice algae models in practice with some physical conditions which influence ecosystem modelling. In the following Chapter, a simple mathematical model to represent the algae population is derived, and analyzed using pseudo spectral numerical methods implemented with MATLAB. The behaviour of the algae population and the boundary layers are discussed by examining the numerical results. Perturbation and asymptotic analysis is used for further analysis of the system using Maple. In the following Chapter a Nutrient Phytoplankton Zooplankton Detritus (or NPZD) model, which is a commonly used type of model in marine ecosystem modelling, is developed based on the framework of Soetaert and Herman. The model is examined under five different experimental setups (herein we mean numerical experiments) and the results are discussed. The NPZD model implemented is compared with a well-studied model in the literature. Our model can be considered somewhat simpler than other models in the literature (though it still has a much larger parameter space than the idealized model discussed in the previous Chapter). Finally we discuss future directions for research.

Acknowledgments

I would like to express my sincere gratitude to my supervisor Prof. Marek Stastna for the guidance and tremendous support specially to improve my MATLAB coding and scientific writing. Thank you for giving me the wonderful opportunity of being a member of your group and all the patience you had when proofreading. Your suggestions and encouragement provided me strength to complete my MSc thesis.

Furthermore I would like to thank the members of the thesis committee, Prof.Sue Ann Campbell and Prof. Francis Poulin.

My special thanks goes to Prof. Achim Kempf who provided his full effort to make my dream a reality to be a graduate student in university of Waterloo. Thank you for your valuable time and continuous support.

My heartiest gratitude goes to my parents for directing me towards education, my brother and my friends for all the caring and support.

Last but not the least I would like to express my deepest appreciation and acknowledgment to my beloved husband for his love and support through out my journey.

Table of Contents

List of Tables

List of Figures

Chapter 1

Introduction

It is a surprising fact to know that algae produce more than 70% of the world's oxygen [9] and they are able to remove vast amounts of carbon dioxide from the atmosphere. Even though the prokaryotic organisms (i.e. organisms, which have no cell nucleus) have been classified as an algae in the past, now they are considered as a bacteria and only the eukaryotic organisms (i.e. organisms, which have a cell nucleus)are considered as true algae. According to the modern definitions true algae are Eukaryotes and they have chloroplasts, which capture light energy to carry out the photosynthesis process [7].

Algae are a huge community of organisms with forms that are unicellular (i.e. that consist of only one cell) and forms that are multicellular (i.e. that consists of multiple cells) [7]. The Euglenophyta or euglenoids (most of which occur in fresh water), the Chrysophyta or the golden-brown algae (occur in both marine and fresh waters, although most species are marine), are unicellular [5]. Chlorophyta (green algae), most of which live in fresh water, although some others are marine. Most green algae are microscopic, but a few species, such as those in the group Cladophora, are multicellular and macroscopic [5]. Some species of green algae include the unicellular Chlamydomonas and Chlorella [5]. The Rhodophyta or red algae are mostly marine algae which are most diverse. The Xanthophyta or yellow-green algae mainly take place in fresh water and unicellular [1]. The Paeophyta or brown algae almost all occur in oceanic environment. These are especially abundant in cool water. Algae of this class are macroscopic in size, and include the giant kelps (a kind of large algae) that can consistently reach tens of meters length [5].

Figure 1.1: Phaeophyta or Brown Algae grow up to 60 meters length. This is multicellular and vegetative (separate from a plant and give rise to a new plant) [1] [4]

Figure 1.2: Rhodophyta or red algae is unicellular and consist of 4000 species with red, purple, black in colors [1] [2]

Algae are more like plants than animals in the sense that they are able to carry out photosynthesis. However, they gain energy from both photosynthesis and the absorbtion of dissolved organic compounds. Various types of algae play significant roles in various

ecosystems. Algae supply food and energy for other aquatic organisms. However, unusual higher levels of algal growth can create obstacles for other lifeforms in the aquatic environment. Moreover, for human use and enjoyment of the aquatic environment, algae can reduce the beauty, clarity and the taste of water. Extremely high levels of algae can prevent sunlight from reaching aquatic plants and will hence limit the growth of plants, or even cause their death. As more algae grow within the lakes, they need to be decomposed by bacteria, which in turn consume dissolved oxygen content in the water. The condition of complete depletion of oxygen is known as anoxia which kills fish and other aquatic creatures. [19].Overhead levels of algae can increase the pH level of water bodies. Photosynthesis will naturally increase the level of pH as a by-product and pH levels are decreased after sunset since the process of photosynthesis ceases. However, extreme fluctuations in pH levels will create stress in a sensitive aquatic environment. High concentrations of algae in drinking water intakes react with chlorine that is used to purify water and can generate cancer causing particles [19]. It is thus very important to understand the population dynamics of algae, both to improve our understanding of the natural world and to realize a proper management strategy that will maintain healthy and natural levels of algae within the aquatic environment.

Obviously algae live and spread in water, but some times they can exist on, and within, ice. The types of algae that can be found in sea ice are commonly known as ice algae. Freezing sea water is different than freezing pure water which gives a firm block of ice. This is because the freezing temperature depends on the salinity of water, and when the salt water concentration is 3.3% the freezing point of arctic sea water reported as $-1.9°C$ [12]. When the temperature reaches the freezing point, sea water begins forming an ice block, with many little channels filled with salt water. Those channels are referred to as brine channels, or brines. Surprisingly, many different types of organisms live in this environment. Ice algae are a class of algae, which have adapted to live in brines. This environment is highly dynamic, often influenced by the weather above the ice, especially when compared to the comparatively stable environment in the underlying sea water.

There are three main factors affecting the growth of ice algae. Temperature, light availability and salinity. The availability of light is the primary influence, with the growth of algae experiencing a proportional increase with the increase in light availability. However above a certain light intensity, algae experience a decline in the growth rate with further increase in light intensity. Somewhat paradoxically, in the Arctic there have been positive and negative correlations reported between algae growth and light availability [15]. In winter almost no light is available and the temperature falls to near $-35°C$ at the upper surface of sea ice and around $-2°C$ in the sea water at the bottom of the sea ice [12]. In summer there is continuous light and the ice temperature is near $0°C$. Light intensity

at the upper surface of sea ice is higher than the bottom surface of sea ice. Accordingly, the structure of brines gets affected and the algae production varies. When temperature decreases, some brine channels freeze, and in those that remain open so that the salinity of the brine increases. As an example, in winter a temperature of $-10°C$ makes salinity in a typical brine channel, rise to 143 PSU (Practical Salinity Units) , estimated as four to five times lager than the salinity of normal sea ice [28]. When the temperature increases in summer, ice melts and the abundant fresh water reduces the salinity in the brine channels. Also increasing temperature make the spatial extent of the brine channels larger (i.e. they grow wider), thereby letting more light in to it. According to an experimental study related to the Arctic sea ice algae, the growth of ice algae happened at temperatures less than $-5.5°C$and a corresponding salinity of 95 PSU [28]. At lower temperatures ($-7.5°C$) and higher salinities (150 PSU) [28] there was no increase in algae, however remaining cells survived.

There was a shocking discovery of massive blooms of algae under the sea ice of the Arctic Ocean in early 2012 by a group of U.S. scientists [29]. Earlier no one believed that a living organism can survive underneath an ice layer which extends to hundreds of kilometers squared in area with insufficient sunlight. Research findings states that algae biomass below the ice surface is four times greater than in open water and it spreads for $>$ 100 km [29] inward from the ice edge, though normally blooms are found along the edge of the ice. This massive growth is hypothesized to be an effect of recent climate change [3]. It has made the ice layer thinner and this allows more light transmission. The authors found the greatest biomass ($>$ 1000 mg cm^{-3}) [29] near the ice water interface and research findings reveal that even though the light under sea ice is much lesser it was sufficient to grow algae under ice twice as fast as in open water [29].

There are many difficulties in carrying out ice algae research in the field, since the sea ice environment is not accessible and even dangerous. Nevertheless, since ice algae are the primary source of food for krill (as well as other marine creatures), and krill provide the main source of food for a diversity of animals at higher trophic levels ice algae is fundamental for the study of Arctic ecosystems. Recently the sea ice loss due to global climate change has become a serious challenge for this flourishing environment. Global warming could decrease, or perhaps eliminate, the space available for the ice algae to grow. This in turn could affect the food cycle of the majority of marine creatures in the Arctic environment.

Figure 1.3: ICESCAPE(Impacts of Climate on Eco Systems and Chemistry of the Arctic Pacific Environment) research scientists experimenting in Arctic sea ice. Climate changes has made the ice layer thinner and melt ponds can be seen which allows more light for the algae to grow underneath ice. [3]

Figure 1.4: Satellite picture of the lake Atitlan. A huge algal bloom which transformed to toxic algae in year 2009 [10]

1.1 What is a model and its purpose

In the natural environment there are many interconnected systems and processes. In order to understand the behaviour of these systems and processes we can use mathematics as a language. The process of forming a system of mathematical equations to illustrate a real life phenomenon using mathematical concepts is known as mathematical modelling [6]. Mathematical models have been used by scientists, research analysts, engineers in order to study the interactions of the system components and predict their behaviour.

A model is a simple way of representing a complex situation. It does not need to consider each and every component involved. Depending on the problem that needs to be solved only the important characteristics are discussed. Most real life problems can be simplified using mathematical modelling as a way to filter out irrelevant information. While the resulting model often cannot be solved exactly, it should at least be "as simple as possible". Many ecological problems cannot be solved without mathematical modelling [20], since the natural world is interconnected and it is impractical to measure all the individual relationships.

1.1.1 Influence of physical conditions on ecosystem models

As mentioned earlier ice algae play an imperative role in the ecosystem. In order to model ice algae it is vital to have awareness of how they will be affected by the changes of the physical environment, and the factors which control algae production. Ice algae production depends on several resources: irradiance which decreases with depth into the ice, nutrients which increase when closer to the ice-water interface, and variations in ice temperature. The natural variability of these quantities is difficult to measure in ice [16]. To develop improved models of algae production it is vital to know how altering environmental conditions effects sea ice, though this is in itself a highly active research topic and will not be pursued in detail in this thesis, though we discuss some literature below.

Lavoie [13] in his paper studies the controlling factors of the growth of the ice which in turn controls the ice algae population. His one dimensional thermodynamic sea ice model, which involves one layer of snow and two layers of ice, explores the significance of the limiting factors on the growth of the ice algae mainly light, nutrients and ice growth rate. It is still uncertain what regulates the oscillation of ice algae populations. According to the studies in [13] ice algal blooms grows exponentially and persist on a constant level, then decline with time. Snow cover, the thickness of ice and self-shading of ice algae all exert some control on the amount of light available near the ice water edge [22]. The model of Pogson [22] provides a lesser light absorption than observations since it only considers the

light from directly above, but the ice base gets light from other directions as well. In order to model light precisely it is necessary to parameterise the thickness of the snow cover since it influences the accumulation of ice algae [22]. According to Lavoie [13] the minimum level of light required for the growth of ice algae is 0.4 μ Einst m^{-2} s^{-1}, though it is likely there is some uncertainty in this value.

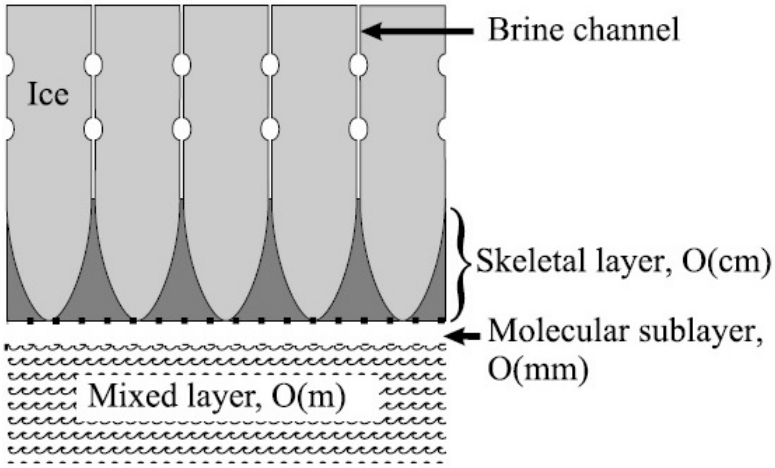

Figure 1.5: Ice algae can be found in the skeletal layer which represent in dark gray [13]

Nitrogen, phosphate and silicon are the main nutrients for the growth of the ice algae [13] but only the silicate concentration is referred to as the limiting nutrient [22] . Figure (1.5) is a rough diagram which shows different layers of the ice base. The ice base consist of thin layers of ice which form the "skeletal layer" or SKL and 95% algae can be find there [13]. The main source of nutrient supply is considered to be the mixed layer [13] [22] and the amount of nutrient fluxes depends on the molecular sub layer thickness which is found adjacent to the bottom of the ice layer. Even though there are other sources of nutrients like brine drainage [13] they are not included in most of the models [13] [22]. Even though it is hard to quantity the amount of nutrients in SKL the value can be predicted from the changes in biomass [13]. However, it is difficult to make accurate measurements of photosynthetic properties over small scale spatial variability. 2D fluorescence imaging is a useful tool in detecting algal biomass over mm-scale variability [16] and this paper discusses the effectiveness of this method on an algae bloom during its initiation in Greenland fast ice. The algae that live closer to ice can access more light but a lesser amount of nutrients. When algal production increases the uptake of nutrients from the SKL increases [13]. Moreover, the supply of nutrients to the SKL also depends on the growth rate of ice. When ice starts to melt (often labelled as "negative growth" of ice) the resulting fresh

water lessens the amount of nutrients found near the ice base [13]. Increased ice growth (positive growth of ice) develops nutrient fluxes [13].

Most of the ice algae are found at the bottom $2-4$ cm [13] [22] [16]. Most of the algae models emphasize basal algae but algae can be found in the ice interior as well [13] [16]. Beyond a certain ice growth rate, algae which are stuck within ice move upward as ice grows [13] [22]. When ice starts to melt algae detach and sink. According to Lavoie [13] the critical ice growth rate for this to occur is between 1.7 cm and 2.9 cm per day and for the negative growth rate it is 1.5 cm per day. In Pogson's multilayer thermodynamic algae model, a coordinate transformation system is used to model this advection part, which in turn allows algae to live and move in between layers, something that was not considered in Lavoie's model.

Depending on the temperature and salinity of sea ice the structure of brine channels varies [22] and the width of the brine channels increases with temperature [16]. With the conditions < 50 psu salinity and $> -2^{\circ}C$ temperature, width of the brine channels increases from nearly $0.3-0.4$ mm and $4-7$ mm [16]. Brine channels provide paths for material, such as nutrients, to travel between ice and sea [22]. Almost all salts and nutrients are melted in brine channels [22] and nitrate and inorganic carbon concentrations in the brine are $3-4$ times higher than in the sea water at the interface of sea and ice [16]. As ice begins to melt in spring, the melt water is flushed out, along with the algae trapped within brine channels [13] [22]. This causes algal bloom decline and therefore it is essential to model brine dynamics for accurate results [22]. The thickness of the snow cover is also a controlling factor for bloom decline since snow cover has an impact on ice melt [22]. A heavier snow cover produces more fresh water and causes more flushing and melt lenses and hence leads to bloom decline. On the other hand, thin snow cover make the sinking of algae quicker. In Pogson's thermodynamic model there was a disparity between modelled and observed speed of the bloom decline. This was explained by hypothesizing that melt water lenses formed under ice and limited the nutrient exchange at the sea-ice interface. Thus the observed algae decline is faster than the modelled result since the modeling of melt water lenses was not included in the model. Ice algae itself also produces heat, as a result of energy gained during the photosynthesis and this process again results in algae loss.

The above discussion clearly shows, that ice algae can be strongly impacted by changing physical conditions. Slight changes to the heat and/or nutrient content can lead to significant changes in the quantity of biomass.

1.1.2 Ice Algae models in practice

The controls of the sea-ice ecosystem are still poorly understood [26]. Since the role of ice algae in the ecosystem is fundamental, forming the bottom of the ecological pyramid, it is necessary to understand and clarify the behaviour of ice algae in order to understand the sea-ice ecosystem. Ice algae models offer better tools to understand the processes that affect ice algae population and controls on this population. In comparison to plankton models, there are very few sea ice algae models that can be discovered when reviewing the literature.

Arrigo (1993) published his ice algae model considering the growth of ice algae as a function of light, temperature, nutrients and salinity. He developed a 2D numerical ecosystem model which studies the primary production in the Antarctic sea ice zone [30]. Arrigo focused on three layers in his sea ice model namely congelation ice which is impermeable except for the system of brine channels, the skeletal layer (SKL) and the platelet ice layer with consolidated crystals. The model simulates the physical properties such as growth of congelation ice and the temporal growth dynamics by solving suitable heat balance equations [30]. Arrigo defines the congelation ice growth rate by considering heat flux from the sea and heat produced by the algae itself. The growth rate of the platelet layer was initially specified as a parameter in the model since it is difficult to define mathematically. Salinity is defined as the balance between the brine trapped within the ice and brine drained through the channels in the ice. The transport of nutrients in the SKL is calculated by the volume of brine flux and the nutrient transport in the platelet layer, both defined using a bulk material transport coefficient [30]. Brine salinity and volume is also computed. The biological properties calculated here are microalgal growth, microalgal respiration, grazing and excretion of algae [30]. The model results verified the fact that the spring bloom is nutrient limited within congelation ice at the beginning, while the bloom is light limited in the bottom platelet layer during the whole process. Arrigo's simulation dramatically describes the physical dynamics of ice growth, structure of ice layers and biological dynamics within ice. More than ten years later Lavioe developed an improved model.

Lavoie (2005) studied a spring algal bloom and his 1D thermodynamic sea ice model consists of one snow layer and two ice layers. This is a simplified version of Arrigo's ice algae model but can be used to study a broader class of limiting factors which control ice algal biomass. This does not include the thickness of the snow since there is a disparity between the measured snow fall and the development of snow carton, may be as a result of wind action [13]. He assumes that silicon is a more important nutrient for ice algal growth and considers its effect in the model. He approximates the light limiting factor using a hyperbolic tangent function and fixes the intensity to 0.4 μ Einst $m^{-2}s^{-1}$ [13] as the benchmark intensity for ice algal growth. The ice algae are confined to the bottom 2 cm

of the ice layer and ice algal growth is studied as a function of light, nutrients and growth rate of ice. This study explores the factors of algae bloom decline in the Canadian Arctic Archipelago with different limitation terms of algal growth and different loss terms [13]. Ice algae detached from ice due to higher rate of ice melting at the bottom ice layer and a melt water lens developed below ice, which limits nutrient supply for the algae. This emphasize the idea that shielding of the ice controls the length of the bloom. Another main focus of this paper is probing the importance of the thickness of the molecular sub layer which limits the supply of nutrients. The model considers more physical processes which effect the model such as heat generated from ice algae itself, effects of varying thickness of the molecular sub layer in limiting nutrients to the SKL, heat and also the amount of algae which is released from the ice and sinks.

Nishi and Tabeta (2006) formed a coupled sea ice ecosystem model and used it to study the role of algae at lake Saroma, Japan. The previous models discussed above do not consider organic carbon emission by ice algae (with possible implications for climate change) [32]. The physical sub model in the ocean model calculates the total heat flux from the surface of water as well as from the atmosphere [32] and the ice model calculates the total heat generated within ice. The biological sub model focuses on biological properties such as photosynthesis, nutrient transport, grazing, excretion, and remineralization [32]. The main idea of this study is to understand the impact of atmospheric heat on the emission of organic carbon from sea ice [32]. The results show that an increase of release of organic carbon depends on the increasing atmospheric temperature and basal ice melting.

Tedesco (2010) introduces a Biologically Active Layer in his study which combines marine ecosystem biology to marine ecosystem physics with a two snow layer-one ice layer-two intermediate layer thermodynamic model [23]. As in the models discussed above, the study of Tedesco does not restrict algae to the bottom 2 cm but considers the fact that ice algae population shows high variability from the beginning of the ice season to the time at which the sea ice starts to melt, and hence is not a layer of constant thickness [23]. The physical model considers two ice layers , one biologically active and one biologically inactive. Past studies have showed that brine volume higher than 5% (permeability threshold value) allows brine channels to be interconnected [23] which in turn facilitates algae accumulation. This ice layer is defined as biologically active. It is assumed that brine volume less than the permeability threshold does not allow algae to grow, and this layer is known as biologically inactive. Both the biologically active and inactive layers have a time varying thickness [23]. The physical model calculates the physical properties of the entire ice layer and the biological model computes the physical properties of biological active layer. The concept of biologically active layer is a useful tool which describes spatial and temporal variability of algal biomass [23].

The study of Pogson (2011) is an improved version of the ice algae model of Lavoie (2005). It couples an ice algae nutrient model with a $1D$ multilayer thermodynamic sea ice model with a focus on the ability of algae to be transported within ice layers [22]. According to Pogson when algae accumulate they divide themselves into layers rather than sticking into one layer. This leads to self-shading and reduction in biomass. This study considers different limiting factors of ice algae such as light, self-shading and snow cover [22]. Pogson's thermodynamic model consist of two components namely a snow and an ice component. Changes of snow-ice thickness, temperature, radiation are calculated as functions of depth. The algae thermodynamic component, which calculates energy absorbed by algae for photosynthesis and energy released as heat, is also computed. The ice algae nutrient model calculates the nutrient concentration in each of the ice layers, as well as nutrient uptake, nutrient and light limiting factors [22]. Pogson's study includes a coordinate transformation which represents the ice algae and nutrient transformation through the ice layers. This model define a critical value for the ice growth rate which allows algae to move up when ice growth rate is lager than the critical value [22]. The controlling factors of the ice algal bloom decline considered in this model are snow cover, ice melt rate and heat flux from sea [22]. The results suggest that ice algae are intensely dependent on the changing ocean conditions such as heat flux, ice melt. Pogson emphasizes the fact that discrepancies of model results and field data were due to selecting constant values for the photosynthetic parameters which change in reality [22]. As a further improvement Pogson suggests to model ice algae in the interior of ice with a more realistic approach.

Chapter 2

Simple models for the algae population

2.1 Explanation of basic models

In the Introduction a variety of rather complicated models of ice algae were discussed. While these have the utility of modelling process that occur in nature, they are generally too complicated for mathematical analysis. In this chapter we adopt a naive mathematical approach based on population dynamics to model ice algae models. The study of population dynamics has a very long history [18]. Mathematical models play an important role in analyzing the changes of population, understanding the range of possible behaviour and for making predictions. The simplest models involve only rate of change of the total population with time and simple growth and death terms. If $P(t)$ is the population at time t the rate of change of population is given by

$$\begin{aligned} \frac{dP}{dt} &= Birth + Death \\ \frac{dP}{dt} &= \alpha P - \beta P \\ P(t) &= P(0)\exp((\alpha-\beta)t) \end{aligned} \tag{2.1}$$

where α and β are positive constants. Here if $\alpha > \beta$ population grows exponentially and if $\alpha < \beta$ it gradually decreases, and in the long run vanishes. The logistic growth model, as well as other more complicated models, can be used to limit possible unbounded growth. We will consider models that assume growth is exponential or logistic. These models do not pay any attention to the spatial distribution, or spatial spread of the species. After

analysing the simplest models we will then move onto models of the change of population that vary in space as a reaction diffusion process, in agreement with most current mathematical models [18].

The remainder of this section presents the simplest models for the algae population in sea ice. The models increase in complexity with each subsection. When possible, the model equations are solved or analyzed by using basic techniques and their weaknesses are discussed. The next section discusses the background of the numerical methods used to obtain numerical solution. Particular attention is paid to Strang splitting methods for reaction diffusion models. Accordingly, both Runge Kutta methods for the reaction terms, and Chebyshev methods for the diffusion terms are discussed. Once the numerical methods tone used are established, the numerical results are discussed. Next, a perturbation analysis is provided for the steady state, demonstrating the existence of an internal boundary layer. Finally, a sensitivity analysis to the model parameters is provided. The primary purpose of the Chapter is to provide a conceptual model of ice algae population dynamics that is much simpler than the field scale models discussed in the previous chapter.

2.1.1 Model with exponential growth

The simplest model for the population growth only depends on birth and death terms, which are proportional to population P(t). In general

$$\frac{\mathrm{d}P}{\mathrm{d}t} = \alpha P - \beta P, \tag{2.2}$$

Where

$P(t)$ is the total population

$\alpha(t)$ is the birth rate, $\alpha(t) > 0$

$\beta(t)$ is the death rate, $\beta(t) > 0$

As a special case where α and β are constants,

$$P(t) = P(0)e^{(\alpha-\beta)t}. \tag{2.3}$$

According to the former result if $\alpha < \beta$, the population decays exponentially with time. On the other hand if $\alpha > \beta$ the population grows exponentially. This is not realistic since unbounded growth is predicted. This model thus needs a modification appropriate for longer time predictions.

2.1.2 Model with logistic growth

As remarked in last section, an exponential model gives unbounded population growth in longer time which is unrealistic. In this kind of a situation the logistic growth in population is more suitable, and is in fact the simplest possible model giving a bounded population for all times.

The logistic model takes the form,

$$\frac{\mathrm{d}P}{\mathrm{d}t} = \alpha P(1 - \frac{P}{P_0}) - \beta P. \tag{2.4}$$

When there is no death term ($\beta = 0$), the logistic model commonly found in textbooks [18] is recovered

$$\frac{\mathrm{d}P}{\mathrm{d}t} = \alpha P(1 - \frac{P}{P_0}). \tag{2.5}$$

where $P_0 > 0$ is the carrying capacity of the environment

Here the carrying capacity is determined by existing resources in the environment. This model has two steady states at $P = 0$ and $P = P_0$, and a simple linear analysis shows that these steady states are unstable and stable steady states, respectively. In terms of the ecosystem, this is to be expected since near the $P = 0$ equilibrium a small, positive population is unaffected by the carrying capacity and hence grows. Similarly near $P = P_0$ the carrying capacity dominates the linear growth rate.

The model can be solved by the following sequence of steps,

$$\begin{aligned} \frac{\mathrm{d}P}{\mathrm{d}t} &= \alpha \frac{P}{P_0}(P_0 - P) \\ \frac{dP}{P(P_0 - P)} &= \frac{\alpha}{P_0} dt \\ \frac{P}{P_0 - P} &= C \exp(\alpha t). \end{aligned} \tag{2.6}$$

where C is a constant.

At $t = 0$, $P(0) = \varepsilon$ gives

$$P(t) = \frac{P_0 \varepsilon \exp(\alpha t)}{P_0 + \varepsilon(\exp(\alpha t) - 1)}. \tag{2.7}$$

The exact solution confirms the conclusion regarding the two steady states reached above. Here $P(t)$ determines a bounded population for all time.

When the death term is there ($\beta \neq 0$) the model equation can be reduced to an identical mathematical form as follows.

$$\begin{aligned} \frac{\mathrm{d}P}{\mathrm{d}t} &= \alpha P(1 - \frac{P}{P_0}) - \beta P \\ \frac{\mathrm{d}P}{\mathrm{d}t} &= (\alpha - \beta)P - \alpha \frac{P^2}{P_0} \\ \frac{\mathrm{d}P}{\mathrm{d}t} &= \tilde{\alpha} P(1 - \frac{P}{\tilde{P}_0}), \end{aligned} \tag{2.8}$$

where

$$\begin{aligned} \tilde{\alpha} &= \alpha - \beta \\ \tilde{P}_0 &= P_0 \frac{\alpha - \beta}{\alpha}. \end{aligned} \tag{2.9}$$

This is in the same form as above when $\beta = 0$. For $\tilde{\alpha} > 0$, $P = 0$ is a unstable equilibrium point and $P = \tilde{P}_0$ is a stable equilibrium point. For $\tilde{\alpha} < 0$, $P \to 0^+$ from above. Therefore this model fails to predict a positive equilibrium when $\tilde{\alpha} < 0$. In the physical environment the sign of $\tilde{\alpha}$ will vary in space. This type of description is discussed in the following subsection.

2.1.3 Model with growth and death rate as a function of depth

The model discussed in the previous subsection fails to predict a positive equilibrium in certain portions of parameter space. In a field situation, whether this is actually the case will depend on a complex interplay between factors that facilitate algae growth (the

availability of sunlight, reasonable temperatures, etc.) and those that lead to ice algae death (excessive cold, lack of sunlight). This observation motivates studying a model with $\tilde{\alpha}$ as a function of depth (z) of the sea ice layer. Before discussing the model, we outline the assumptions made in deriving the model. Assume $z = 0$ is at the top of the upper surface of the ice and z increases downward. At the upper surface there is more light and generally a lower temperature compared to the bottom surface. Therefore algae grow faster as well as die off faster. This implies α is large but $\beta > \alpha$. At the bottom surface there is less light, but the temperature is warmer compared to to the upper surface, due to the proximity to liquid water. This implies α is small, however β can be expected to be even smaller. We thus assume β decays faster than α with depth. Let's assume

$$\begin{aligned} \alpha(z) &= \frac{\alpha_0}{z} \\ \beta(z) &= \frac{\beta_0}{z^2}. \end{aligned} \tag{2.10}$$

Here $\alpha_0, \beta_0 > 0$. According to the chosen α and β,

$$\tilde{\alpha}(z) = \frac{\alpha_0}{z} - \frac{\beta_0}{z^2}, \tag{2.11}$$

and

$$\begin{aligned} \tilde{P}_0 &= P_0 \frac{\alpha - \beta}{\alpha} \\ \tilde{P}_0 &= P_0 \left(\frac{\frac{\alpha_0}{z} - \frac{\beta_0}{z^2}}{\frac{\alpha_0}{z}} \right) \\ \tilde{P}_0 &= P_0 \left(1 - \frac{\beta_0}{\alpha_0 z} \right). \end{aligned} \tag{2.12}$$

Consider $\tilde{\alpha} = 0$. Then,

$$\begin{aligned} \frac{\alpha_0}{z} - \frac{\beta_0}{z^2} &= 0 \\ z &= \frac{\beta_0}{\alpha_0} \end{aligned} \tag{2.13}$$

When this is the case the equation (2.12) becomes,

$$\tilde{P}_0(z = \frac{\beta_0}{\alpha_0}) \quad = \quad 0. \tag{2.14}$$

This verifies the natural behavior of the population when β dominates α, $P = 0$ at $z = \frac{\beta_0}{\alpha_0}$. On the other hand as $z \to 0$ from above the equation (2.11) becomes,

$$\tilde{\alpha}(z) \quad = \quad O(\frac{1}{z^2}) < 0. \tag{2.15}$$

This shows that model is singular near $z = 0$. To obtain a model that remains regular near $z = 0$ we need to define α and β in a different way. Let's move on to a model assuming that α and β decay by a fixed percent at regular intervals of depth z. Therefore α and β can be defined as an exponential decay.

$$\begin{aligned} \alpha &= \alpha_0 \exp(\frac{-z}{L_\alpha}) \\ \beta &= \beta_0 \exp(\frac{-z}{L_\beta}). \end{aligned} \tag{2.16}$$

Relevant to the above,

At $z = 0$, $\alpha = \alpha_0$ and $\beta = \beta_0$.

To set $\tilde{\alpha} < 0$ at $z = 0$, need $\beta_0 > \alpha_0$.

To ensure that β falls faster than α, we need to set $L_\beta < L_\alpha$.
According to the chosen α and β as in (2.16),

$$\tilde{\alpha} \quad = \quad \alpha_0 \exp(\frac{-z}{L_\alpha}) - \beta_0 \exp(\frac{-z}{L_\beta}). \tag{2.17}$$

When $\tilde{\alpha} = 0$ there is no population growth and if we label the depth where this occurs as z_*, we find

$$\begin{aligned} \alpha_0 \exp(\frac{-z_*}{L_\alpha}) &= \beta_0 \exp(\frac{-z_*}{L_\beta}) \\ z_* &= (\frac{L_\beta L_\alpha}{L_\alpha - L_\beta}) \ln(\frac{\beta_0}{\alpha_0}) > 0. \end{aligned} \tag{2.18}$$

For $z > z_* > 0$ and $\tilde{\alpha} > 0$ the system tends to the equilibrium.

$$\begin{aligned} \tilde{P_0} &= P_0 \frac{\alpha - \beta}{\alpha} \\ \tilde{P_0} &= \frac{\alpha_0 \exp(\frac{-z}{L_\alpha}) - \beta_0 \exp(\frac{-z}{L_\beta})}{\alpha_0 \exp(\frac{-z}{L_\alpha})} P_0 \\ \tilde{P_0} &= (1 - \frac{\beta_0}{\alpha_0} \exp(-z(\frac{1}{L_\beta} - \frac{1}{L_\alpha})))P_0. \end{aligned} \tag{2.19}$$

Here $\frac{1}{L_\beta} - \frac{1}{L_\alpha} > 0$ and as $z \to \infty$, $\tilde{P_0} \to P_0$.

Moreover

$$\frac{\mathrm{d}\tilde{P_0}}{\mathrm{d}z} > 0$$

and so the equilibrium population increases with depth, for $z > z^*$. Let's consider $\tilde{P_0}$ at z_*.

$$\begin{aligned} \tilde{P_0}(z_*) &= (1 - \frac{\beta_0}{\alpha_0} \exp(\ln(\frac{\beta_0}{\alpha_0})))P_0 \\ \tilde{P_0}(z_*) &= (1-1)P_0 = 0. \end{aligned} \tag{2.20}$$

This confirms that when $\alpha - \beta = 0$ the equilibrium population goes to zero. Figure (2.1) displays $\tilde{\alpha}$ and how the population P varies with the depth z.

The above results demonstrate that the model remains regular at the top of the ice layer and it predicts a zero population for $0 \leq z \leq z^*$, the region where $\alpha - \beta < 0$. For $z > z^*$ the population will grow with increasing equilibrium population. Thus to summarize, the logistic growth model with spatially variable growth rate and death rate is more consistent with the natural environment. However, this model does not consider the physical spatial spread of the population. Therefore the model should be augmented. It should be noted that in the above there is no mechanism by which organisms change their depth (z) and thus z dependence is parametric only and a local stability analysis is thus valid.

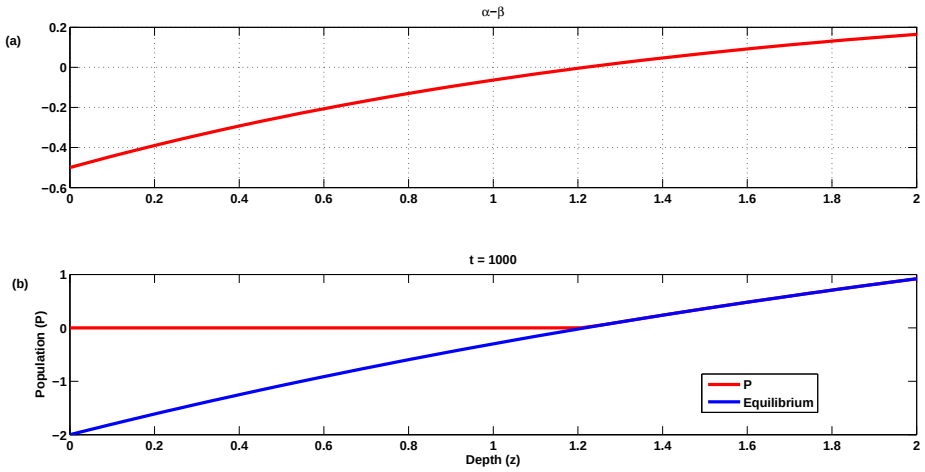

Figure 2.1: The difference of growth rate and death rate (top) and changes in population with the depth (bottom)

2.1.4 Model with diffusion

The minimal rational model of ice algae population will include both the spatially dependent birth and death parameters associated with a spatially varying distribution of light, temperature and nutrients, and the natural spreading of the population in space. In agreement with the mathematical literature, [18]., this model consists of a logistic model to describe the population dynamics and a diffusion term to describe the spatial spread of population,

$$\begin{aligned} \frac{\partial P}{\partial t} &= \kappa \frac{\partial^2 P}{\partial z^2} + (\alpha - \beta)P - \frac{\alpha P^2}{P_0}, t > 0, x \in (0, L) \\ P(z = 0, t) &= P_z(z = L, t) = 0 \\ P(z, t = 0) &= f(z, t) \end{aligned} \tag{2.21}$$

Since it is very cold on the surface, boundary condition on the surface of ice is $P = 0$ and no flux of population at $z = L$.

Here κ denotes the diffusion coefficient, which in a fluid environment can be thought of as being set by the fluid turbulence.

$$\begin{aligned} \alpha &= \alpha_0 \exp(\frac{-z}{L_\alpha}) \\ \beta &= \beta_0 \exp(\frac{-z}{L_\beta}) \end{aligned} \tag{2.22}$$

Here α and β are defined as exponentially decaying functions based on the assumption that α and β decreasing by a fixed percent at regular intervals of depth z. Equation (2.21) is impossible to solve analytically. It is thus appropriate to solve it numerically. The details of the numerical methods are discussed in the following subsection. One of the things numerical models will be able to tell us is whether the naive stability analysis based on the reactive equilibrium carries over to the case with diffusion.

2.2 Description of Numerical Methods

This section discusses the background necessary to obtain the numerical solution of reaction diffusion equations. It is well known [17] that diffusion problems require implicit methods to maintain a reasonable time step (unless the diffusivity is very small in which case an explicit scheme may be possible). However, the logistic growth term in (2.21) is nonlinear and as such is more conveniently treated by an explicit scheme. The reconciliation between these two methods is referred to as the Strang splitting method.

2.2.1 Strang splitting method

This method splits the governing equation into several parts which are solved independently on the time intervals $[t_n, t_{n+1}]$. Time splitting methods, or fractional step methods, create splitting errors in each time step. Even with exact integration of each subpart the final result will be only first order accurate. This has been improved to second order accuracy with Strang splitting method [17].

Conceptually, splitting can be thought of as solving the ordinary differential equation for the reaction,

$$\frac{dP}{dt} = (\alpha - \beta)\, P - \frac{\alpha P^2}{P_0}. \tag{2.23}$$

and the partial differential equation for the diffusion

$$\frac{\partial P}{\partial t} = \kappa \frac{\partial^2 P}{\partial z^2}. \tag{2.24}$$

The idea of the Strang splitting method is to solve the first part (2.23) for a half time step, then the result obtained is use to solve the second part (2.24) over a full time step and this result is used to solve the first part (2.23) again for another half a time step.

There are many methods to numerically solve an ordinary differential equation in practice. Euler's method is the simplest numerical algorithm, but it is generally not recommended in practical situations [14]. Note however, that Euler's method is really important since most of other advanced numerical methods are derived using the same idea as Euler's method (i.e. Taylor series). There are multi step methods as well as multistage methods in practice to solve an ODE [17]. Multi step methods use values of solutions calculated at previous time levels (P^n, P^{n-1}, P^{n-2} etc.) to approximate P^{n+1}. This can give high order of accuracy when using polynomial interpolation with high order polynomials [27]. In order to obtain high order of accuracy with one step methods like Runge-Kutta it is essential to use a multi stage method [17]. Multi stage methods calculate several in between values of the solution in each time step. Below is the derivation of second order two stage Runge Kutta method as an extension of Euler's method.

2.2.2 Runge-Kutta method

In general assume

$$\frac{\mathrm{d}P}{\mathrm{d}t} = f(t, P(t)). \tag{2.25}$$

Then use the Euler's method to approximate the value $P(t_n + 0.5\Delta t)$ which is for a half of a time step.

$$P^* = P^n + 0.5\Delta t f(t, P^n). \tag{2.26}$$

For the next step use this result to approximate $P(t_n + \Delta t)$ which is for a full time step as follows.

$$P^{n+1} = P^n + \Delta t f(P^n + 0.5\Delta t f(t, P^n)). \tag{2.27}$$

This is second order accurate (and is sometimes referred to as the midpoint rule). (Refer chapter 6 of Finite Difference Methods for Differential Equations [17] for further details). The fourth-order Runge-Kutta method is an extension of the idea presented above, and

advances the solution through four sub-steps and combines these evaluations to achieve fourth order accuracy at each time step [14].

In general, in order to solve the equation (2.23)

$$\frac{\mathrm{d}P}{\mathrm{d}t} = (\alpha - \beta)\, P - \frac{\alpha P^2}{P_0} = f(t, P(t)), \tag{2.28}$$

fourth-order Runge-Kutta method requires us to calculate,

$$\begin{aligned} K_1 &= \Delta t f(t^n, P^n) \\ K_2 &= \Delta t f(t^n + \frac{\Delta t}{2}, P^n + \frac{K_1}{2}) \\ K_3 &= \Delta t f(t^n + \frac{\Delta t}{2}, P^n + \frac{K_2}{2}) \\ K_4 &= \Delta t f(t^n + \Delta t, P^n + K_3) \\ P^{n+1} &= P^n + \frac{K_1}{6} + \frac{K_2}{3} + \frac{K_3}{3} + \frac{K_4}{6} + O(\Delta t^5), \end{aligned} \tag{2.29}$$

where Δt is the step size and the superscript n denotes the number of iteration.

2.2.3 Numerical solutions of the diffusion equation and stability analysis

Various numerical schemes are discussed in standard books like [17], [31] to find numerical solutions of the diffusion equation (2.24). Below provides a overview of numerical solutions to diffusion equation using the finite difference method. Use centered difference in space and a forward difference in time to discretize the diffusion equation (2.24) as follows,

$$\begin{aligned} \frac{P_j^{n+1} - P_j^n}{\Delta t} &= \frac{1}{\Delta x^2}(P_{j+1}^n - 2P_j^n + P_{j-1}^n) \\ P_j^{n+1} &= P_j^n + \frac{\Delta t}{\Delta x^2}(P_{j+1}^n - 2P_j^n + P_{j-1}^n). \end{aligned} \tag{2.30}$$

This is an explicit scheme since the values calculated at previous time levels are used to calculate P^{n+1}. Von Neumann analysis can be used to analyze the stability since (2.24)

is a constant coefficient linear PDE [17]. The Von Neumann analysis [17] (chapter 12) for (2.30) gives the requirement for stability as,

$$\frac{\Delta t}{\Delta x^2} \leq \frac{1}{2}. \tag{2.31}$$

The above equation (2.31) displays the stability condition for the equation(2.24) using an explicit scheme. This forces the time step to be too small for practical use (though in one dimension this could be done since the memory requirements are small), in order to have a stable solution. Therefore this is not an efficient method to solve the diffusion equation. Other well known [17] methods are the implicit, or backward Euler method, or the Crank Nicholson method. These are first and second order method, respectively. Both methods are unconditionally stable, or in other words stable for any choice of Δt and Δx. This can be proved using Von Neumann analysis. Further details can be found in [17] (chapter 12).

2.2.4 Chebyshev method for spatial discretization

The results of the Runge-Kutta scheme presented above can be used to step the reaction part of the governing equation forward, while an implicit scheme can be used to advance the partial differential equation (2.24) forward in time. However, the spatial derivatives must be discretized as well. While finite difference schemes are commonly discussed in textbooks [17], it is possible to derive methods whose order of accuracy increases with the number of grid points. These are known as Chebyshev pseudo spectral methods and an outline of their use is presented below. For details see chapter 6 of the textbook "Spectral Methods in Matlab" [27].

To approximate the derivative of a function with spectral accuracy on a periodic domain, trigonometric polynomials on uniform grids are used [27] (chapter 1). For non periodic problems algebraic polynomials on unevenly spaced grid are necessary [27] (chapter 1). The Chebyshev method is a spectral collocation method which interpolates given data on a set of grid points with a polynomial, finds the derivative of the interpolating polynomial, and finally evaluates the derivative at the grid points. The set of Chebyshev points is given by [27]

$$x_j \;=\; \cos(j\pi/N)\;, \qquad j = 0, 1, ..., N, \tag{2.32}$$

while the Chebyshev differentiation matrix is defined as,

$$(D_N)_{ij} = \frac{c_i}{c_j}\frac{(-1)^{i+j}}{x_i - x_j},\ i \neq j, \quad i,j = 0, ..., N, \tag{2.33}$$

where

$$c_i = \begin{cases} 2, & i = 0 \text{ or } N \\ 1, & \text{otherwise} \end{cases}$$

for the off diagonal elements and

$$(D_N)_{ii} = -\sum_{j=0, j\neq i}^{N} (D_N)_{ij}, \tag{2.34}$$

for the diagonal elements.

2.2.5 Numerical solutions of the PDE

To obtain a numerical approximation for the PDE we used the backward difference formula at time t_{n+1} for the time derivative and the Chebyshev spectral method for the spatial derivative. In MATLAB, the function cheb [27](page 54) is used to obtain the Chebyshev grid and the differentiation matrix.

$$\begin{aligned} \frac{\partial P}{\partial t} &= \kappa \frac{\partial^2 P}{\partial z^2}. \\ \frac{P^{n+1} - P^n}{\Delta t} &= \kappa D^2 P^{n+1} \\ (I - \kappa D^2 \Delta t) P^{n+1} &= P^n. \end{aligned} \tag{2.35}$$

Here D denotes the Chebyshev differentiation matrix and I denotes the identity matrix. The second derivative is calculated by squaring the differentiation matrix D. As the next step we need to impose the boundary conditions. According to Trefethen [27] chapter 13, to enforce the Dirichlet boundary conditions remove the last row and last column. On the other hand since we have a Neumann boundary condition at the right end point use the differentiation matrix to replace the first row. This means $(n-1)$ rows of the matrix $(I - \kappa D^2 \Delta t)$ of the system of equations will calculated from D^2 and one row from D.

Equation (2.35) can be solved implicitly for P^{n+1} and this can be again used to solve the ODE (2.23) for a half of a time step.

2.2.6 Numerical solutions of the Reaction Diffusion Equation

The complete algorithm for the numerical solutions of the reaction diffusion equation is thus given by the following series of steps. From equation (2.29)

$$\begin{aligned} K_1 &= 0.5\Delta t f(t^n, P^n) \\ K_2 &= 0.5\Delta t f(t^n + \frac{\Delta t}{4}, P^n + \frac{K_1}{2}) \\ K_3 &= 0.5\Delta t f(t^n + \frac{\Delta t}{4}, P^n + \frac{K_2}{2}) \\ K_4 &= 0.5\Delta t f(t^n + \frac{\Delta t}{2}, P^n + K_3) \\ P_*^{n+1} &= P^n + \frac{K_1}{6} + \frac{K_2}{3} + \frac{K_3}{3} + \frac{K_4}{6} + O((\frac{\Delta t}{2})^5). \end{aligned} \tag{2.36}$$

From equation (2.35)

$$(I - \kappa D^2 \Delta t) P_{**}^{n+1} = P_*^{n+1}. \tag{2.37}$$

Again using the equation (2.29)

$$\begin{aligned} K_1^{'} &= 0.5\Delta t f(t^n, P_{**}^{n+1}) \\ K_2^{'} &= 0.5\Delta t f(t^n + \frac{\Delta t}{4}, P_{**}^{n+1} + \frac{K_1^{'}}{2}) \\ K_3^{'} &= 0.5\Delta t f(t^n + \frac{\Delta t}{4}, P_{**}^{n+1} + \frac{K_2^{'}}{2}) \\ K_4^{'} &= 0.5\Delta t f(t^n + \frac{\Delta t}{2}, P_{**}^{n+1} + K_3^{'}) \\ P^{n+1} &= P_{**}^{n+1} + \frac{K_1^{'}}{6} + \frac{K_2^{'}}{3} + \frac{K_3^{'}}{3} + \frac{K_4^{'}}{6} + O((\frac{\Delta t}{2})^5). \end{aligned} \tag{2.38}$$

After a finite number of iterations P^{n+1} is the numerical solution of the reaction diffusion equation (2.21) obtained from the above described numerical methods.

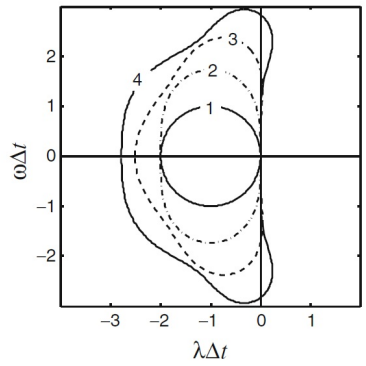

Figure 2.2: Absolute stability regions for explicit Runge Kutta schemes of orders 1 to 4 [31]

As we discussed above an appropriate time step is crucial for a numerical method to be stable. Numerical solutions to the equation (2.23) with a appropriate value of Δt are called absolutely stable if $|P^n| \leq |P^0|$ for all n [31].

Figure (2.2) displays the absolute stability regions for the explicit Range Kutta scheme. For the each case of order 1 to 4 of explicit Range Kutta Scheme the absolute stability region indicated within the curve [31]. Refer chapter 2 of [31] for a more detailed discussion.

The above described numerical methods have been coded up, and the resulting numerical solutions have been analyzed using MATLAB. The following Section,(2.3), discusses these results.

2.3 Numerical Results

The content here describes the numerical solutions for the equation (2.21) discussed above. The equation is solved using fourth order explicit Range Kutta scheme for the reaction, implicit time stepping for the diffusion, with Strang splitting, as described in section (2.2). The numerical solution we get for the population $P(z,t)$ is graphed in several ways to analyze the reaction diffusion model.

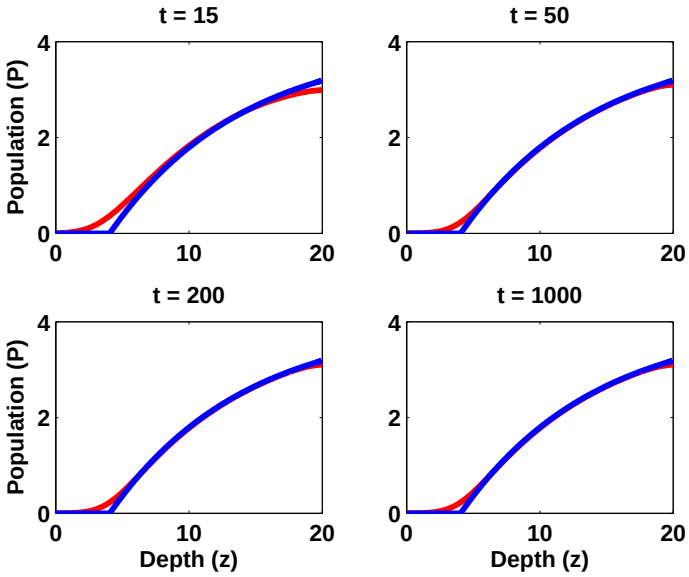

Figure 2.3: (a) Population (P) dynamics as the depth (z) varies using reaction diffusion model. Here $\alpha = \exp\left(-\frac{z}{10}\right)$, $\beta = 1.5\exp\left(-\frac{z}{5}\right)$. Population is zero when $\alpha - \beta < 0$ and the population (red) increases and reaches the reactive equilibrium (blue) when $\alpha - \beta > 0$. The initial condition consists of a small random perturbation of the zero equilibrium.

Figure (2.3) illustrates how the population $P(z,t)$ changes with time and approaches the equilibrium related to the chosen α, β and a constant diffusion coefficient ($\kappa = 1\times10^{-3}$). The bottom right panel of the figure (2.3) shows the population distribution when it has essentially reached a steady state. According to the chosen α and β the population is zero within the range of $\tilde{\alpha} = \alpha - \beta < 0$ and when $\tilde{\alpha} = \alpha - \beta > 0$ the population grow towards the equilibrium, but diffusion modifies the steady state value from that predicted by the ODE theory.

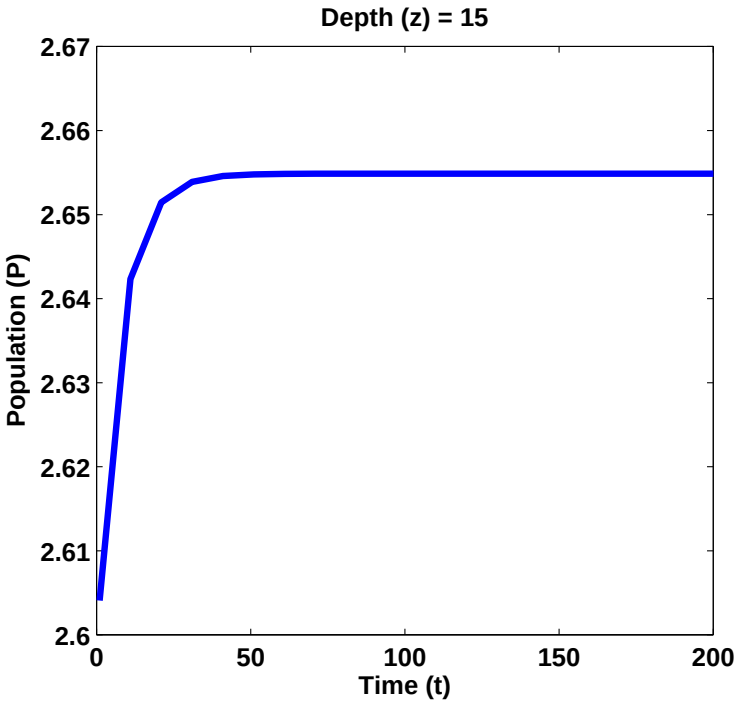

Figure 2.4: Population distribution at $z = 15$. Here $\alpha = \exp\left(\frac{-z}{10}\right)$, $\beta = 1.5\exp\left(\frac{-z}{5}\right)$. Population increase initially then become constant.

Lets consider the growth of population near the bottom layer of ice. Figure (2.4) shows the population distribution at a fixed depth ($z = 15$). Initially population grow and eventually becomes constant with time.

Figure (2.5) illustrates the effect of change in the strength of diffusion, or in other words changing κ. For small values of the diffusion coefficient a stable non-zero solution is established and this solution matches the prediction of the governing ODE for a pure reaction system ($\kappa = 0$). In contrast, for larger diffusion coefficient, the solution deviates from the reactive equilibrium. Essentially, it is smoother and controlled to a greater degree by the boundary conditions. According to figure (2.5), for very large values of diffusion coefficient κ, the population will tend towards $P = 0$ and become absorbed (basically due to the Dirichlet condition at the surface), hence P = 0 is a stable steady state in the high diffusion limit.

There is another significant insight that we gain from the figure (2.5) for smaller values of κ. This shows that there is a region near z^* and near the right boundary where the solution changes rapidly. These are called boundary layers [24]. There are two boundary

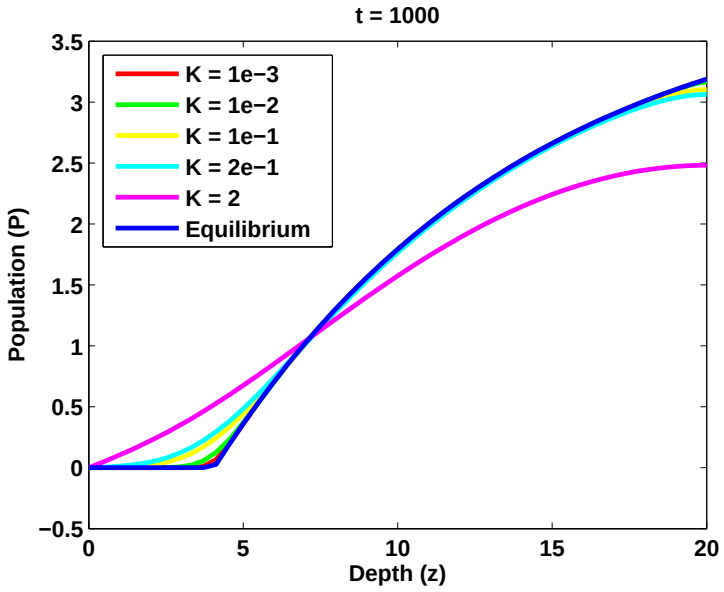

Figure 2.5: Steady state population dynamics for different values of Kappa. Here $\alpha = \exp\left(\frac{-z}{10}\right)$, $\beta = 1.5\exp\left(\frac{-z}{5}\right)$. Population deviates from the equilibrium for large diffusion coefficients and reach the equilibrium for smaller diffusion coefficients.

layers that need to be analyzed, one near z^* and one near the right boundary where $\frac{\partial P}{\partial z} = 0$. The thickness of each boundary layer region depends on the diffusion coefficient and numerical methods can be used to get an idea of how this region of boundary layers behaves as κ changes. The following methodology is used to measure the thickness of the boundary layer regions in which the diffusive region is different from the ODE steady state.

In this case the differences between the value of population and purely reactive equilibrium was calculated and graphed as the first step. Figure (2.6) shows there are two peaks; at the right boundary and at the point where corner of the equilibrium placed as a result of the boundary layers. In order to measure the thickness of the boundary layers it is easy to get the half width of the peaks.

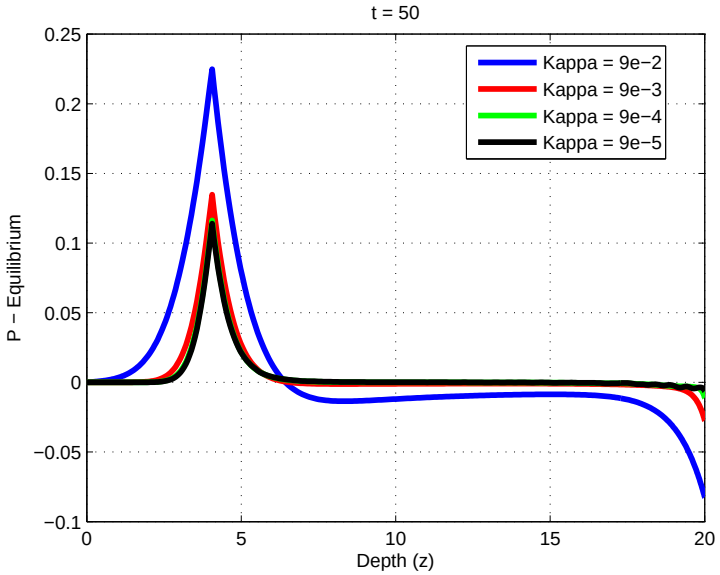

Figure 2.6: Difference of population and the equilibrium for different values of diffusion coefficients. The two peaks at the right boundary and at z^* are the results of boundary layers at the two points.

The difference of population and equilibrium was scaled by the maximum value of the difference for ease of the calculations. The intermediate peak was considered first which relates to the internal boundary layer at the corner. Related values of depth were calculated where the scaled difference is one (at the peak) and at the place where the scaled difference is equal to 0.5. The half width is calculated by the difference of values of depth obtained above. Note that the half width is always positive so the absolute value of the difference was taken.

Since

$$\begin{aligned} L_c &\sim \kappa^p \\ L_b &\sim \kappa^q \end{aligned} \tag{2.39}$$

where L_c and L_b are the width of the peaks at the corner and the boundary respectively. Therefore the half width of the peak can be determined as a function of κ. Once the half width is calculated the logarithm value of half width graphed with logarithm value of κ. According to the equation (2.39), the slope of the graph should give the value of

power p. If the computation is carried out for long times, the predicted value is essentially time dependent and provides an estimate for how boundary layer thickness scales with diffusivity.

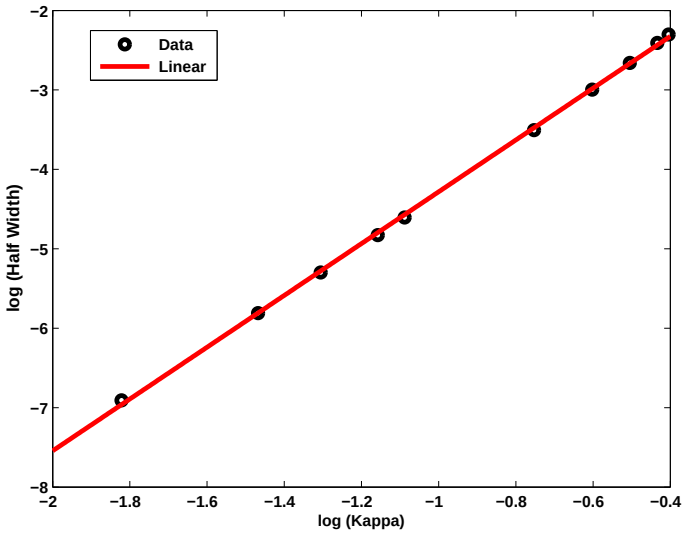

Figure 2.7: Log of half widths of the boundary layer at the corner of the equilibrium, for different values of Kappa. The linear data fit of the form $p_1 x + p_2$ is with the coefficients $p_1 = 3.2611$, $p_2 = -1.0213$, norm of residuals (r) $= 0.092545$

Figure (2.7) displays a best linear fit where the slope of curve should give the value of the power of κ at the corner. The slope of the linear fit is 3.2611.

The region near the right boundary can also be analyzed in the same way in order to get an estimate for the width of the boundary layer. The difference of population and equilibrium was scaled by the value at bottom boundary. Half width for the boundary layer at the right end is calculated using the same method as above. Base on the equation (2.39), the slope of the graph should give the value of power q.

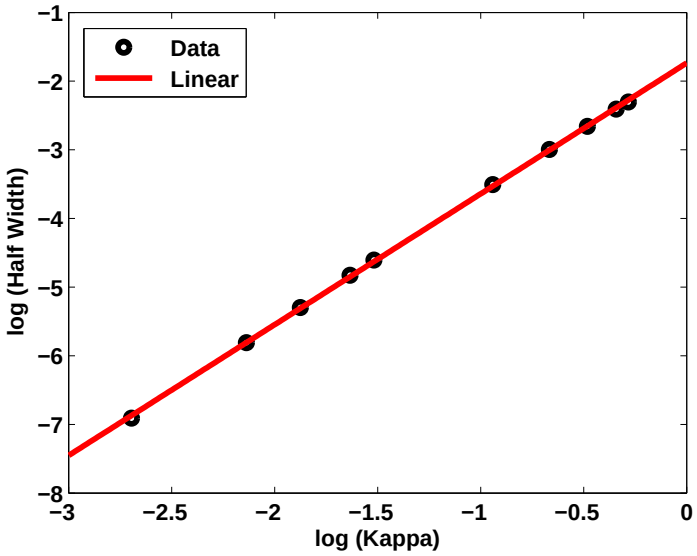

Figure 2.8: Log values of half widths of the boundary layer at the right boundary, for different values of Kappa. The gradient of this graph gives the value of the power q. The linear data fit of the form $p_1 x + p_2$ is with the coefficients $p_1 = 1.905$, $p_2 = -1.7361$, norm of the residual is (r) = 0.065714

According to the figure (2.8) the power of κ near the right boundary is 1.905. The boundary layers are analyzed in more detail using Pertubation theory in the next section (2.4).

2.4 Perturbation Theory and Asymptotic Analysis

While we have solved the reaction diffusion model numerically, it can also be understood using perturbation theory. This is accomplished in this subsection using modified, simpler problems. Perturbation theory includes various techniques of finding an approximate solution to a problem which is impossible to solve analytically. These develop a series expansion in terms of a small parameter and the first few terms of the series give an approximation to the solution.

As a first step the Reaction Diffusion model (2.21) can be solved by regular perturbation theory. The idea here is to start with the full form of the equation and expand it in terms of the small parameter $\kappa = \varepsilon$.

We then look for a solution as a Taylor series in ε.

$$P(\varepsilon) = P^{(0)} + P^{(1)}\varepsilon + O(\varepsilon^2). \tag{2.40}$$

$O(1)$ problem :

$$\frac{\partial P^{(0)}}{\partial t} = (\alpha - \beta)P^0 - \frac{\alpha}{P_0}(P^{(0)})^2, \tag{2.41}$$

with the initial condition and boundary conditions,

$$\begin{aligned} P^{(0)}(z=0) &= 0 \\ P_z^{(0)}(z=L) &= 0 \\ P^{(0)}(t=0) &= f(z). \end{aligned} \tag{2.42}$$

The leading order solution is,

$$P^{(0)} = \frac{\tilde{P}_0 f(z)\exp(\tilde{\alpha}t)}{\tilde{P}_0 + f(z)(\exp(\tilde{\alpha}t) - 1)}, \tag{2.43}$$

where $\tilde{\alpha} = \alpha - \beta$ and $\tilde{P}_0 = P_0\frac{\alpha-\beta}{\alpha}$.

The leading order solution obviously satisfies the initial condition and Dirichlet boundary condition at $z = 0$ according to the choice of α and β. But $P_z^{(0)}(L) \neq 0$, hence it does not satisfy the Neumann boundary condition at the right end. Also, the solution does not have a derivative at z^* so cannot satisfy the steady state PDE. Zero Neumann boundary conditions specify that either the population is isolated (with no incoming or outgoing flow of organisms) or else the population stays in a dynamic balance with the inflow or outflow of individuals at the boundaries [31]. Thus it can be expected a boundary layer will exist at the right boundary and a second boundary layer will exist at the corner ($z = z^*$) where the change of stability occurs. This implies that the solution obtained from regular perturbation theory is only an outer solution and an inner solution must be found.

In order to make the algebra as simple as possible we modify the original problem to look at each type of boundary layer on its own. In particular we will find it easier to work with a situation where the boundary layer occurs at $z = 0$.

$$\varepsilon\frac{\mathrm{d}^2P}{\mathrm{d}z^2} - (P - (1 - z)) = 0, \tag{2.44}$$

where

$$P(1) = 0 \text{ and } P_z(0) = 0. \tag{2.45}$$

The model equation presented above captures what happens near the bottom of the ice where a Neumann boundary condition is imposed, but $\alpha > \beta$ so we get a non-trivial equilibrium. The equation is constructed so that it has an exact solution and satisfies the boundary condition. The solution reads as,

$$P(z) = \frac{e^{\frac{z}{\sqrt{\varepsilon}}} e^{-\frac{1}{\sqrt{\varepsilon}}} \sqrt{\varepsilon}}{e^{\frac{1}{\sqrt{\varepsilon}}} + e^{-\frac{1}{\sqrt{\varepsilon}}}} - \frac{e^{\frac{-z}{\sqrt{\varepsilon}}} e^{\frac{1}{\sqrt{\varepsilon}}} \sqrt{\varepsilon}}{e^{\frac{1}{\sqrt{\varepsilon}}} + e^{-\frac{1}{\sqrt{\varepsilon}}}} - z + 1. \tag{2.46}$$

Maple can be used to analyze the exact solution for the boundary layer near $z = 0$. Below is the illustration of the result of the model equation (2.44) with the boundary conditions (2.45).

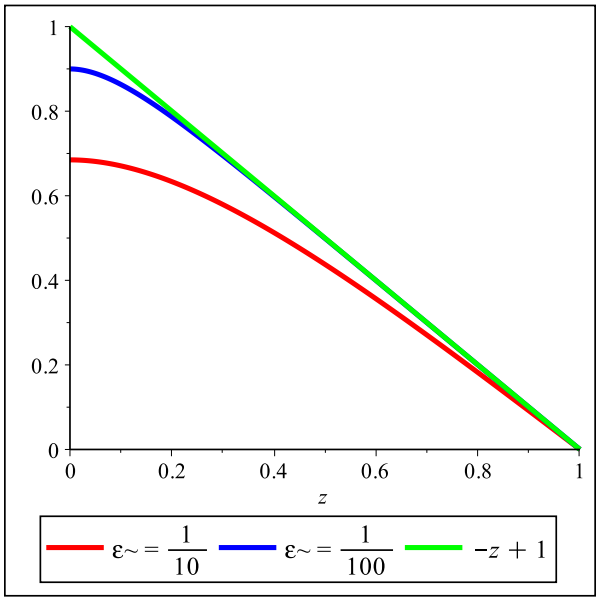

Figure 2.9: Exact solution to the model DE (2.46) that captures behavior near the bottom of the ice with Neumann boundary condition. Horizontal axis has the values of depth and vertical axis represent the values of population.

Figure (2.9) shows the behaviour of the exact solution (2.46) for two different ε along with the outer solution $1-z$. The rate of change of population starts from zero at the left endpoint. The solution, however, rapidly tends to the outer solution $1-z$. In order to look at the boundary layer thickness we subtract the outer solution from the exact solution (2.46). Then the inner solution reads

$$P_{in}(z) = \frac{e^{\frac{z}{\sqrt{\varepsilon}}}e^{-\frac{1}{\sqrt{\varepsilon}}}\sqrt{\varepsilon}}{e^{\frac{1}{\sqrt{\varepsilon}}}+e^{-\frac{1}{\sqrt{\varepsilon}}}} - \frac{e^{\frac{-z}{\sqrt{\varepsilon}}}e^{\frac{1}{\sqrt{\varepsilon}}}\sqrt{\varepsilon}}{e^{\frac{1}{\sqrt{\varepsilon}}}+e^{-\frac{1}{\sqrt{\varepsilon}}}}. \tag{2.47}$$

The inner solution can be scaled so that its maximum is one, and this scaled solution reads

$$P_{in\_scaled}(z) = \frac{\left|e^{\frac{-1+z}{\varepsilon}} - e^{-\frac{(-1+z)}{\varepsilon}}\right| e^{\frac{1}{\sqrt{\varepsilon}}}}{-1+e^{\frac{2}{\sqrt{\varepsilon}}}}, \tag{2.48}$$

and can be expanded in a series about $z=0$, since the boundary layer is presumably thin.

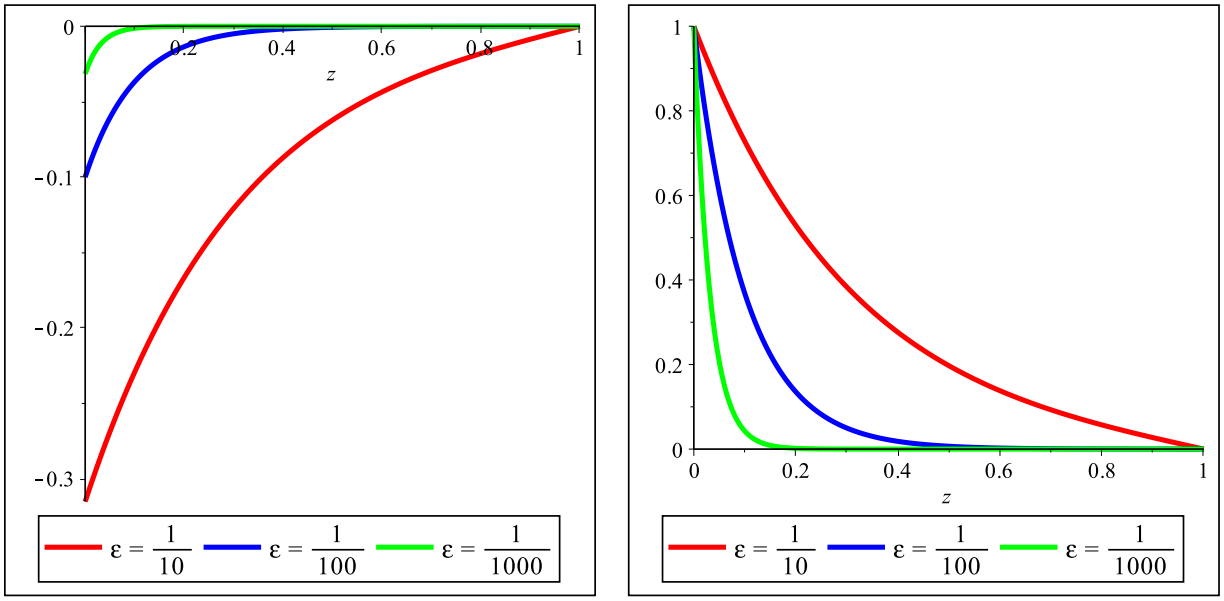

Figure 2.10: Left side graph represent the inner boundary layer solution (2.47) near $z=0$ for three different ε's. Right side graph represents the scaled boundary layer to its maximum (2.48).

The linear approximation for the scaled inner solution is as follows.

$$P_{in\_scaled}(z) \quad = \quad 1 - \frac{e^{\frac{2}{\sqrt{\varepsilon}}} + 1}{\sqrt{\varepsilon}(-1 + e^{\frac{2}{\sqrt{\varepsilon}}})} z + O(z^2). \tag{2.49}$$

Below figure (2.11) shows how the leading polynomial of the equation (2.49), approximates the scaled inner solution.

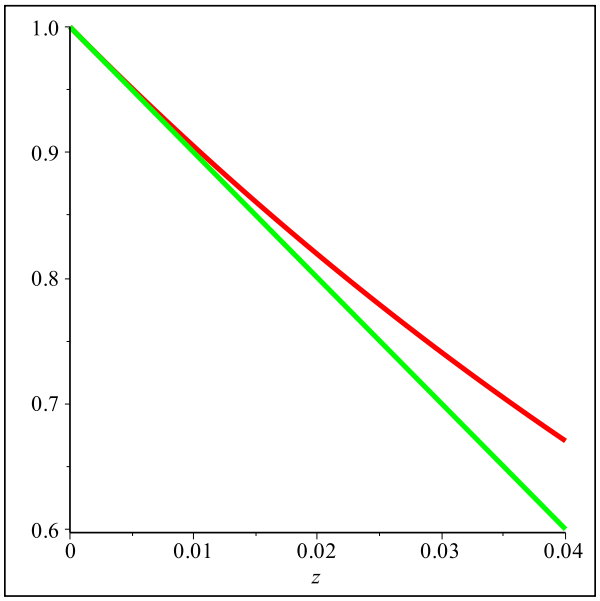

Figure 2.11: The leading order of the linear approximation to the scaled boundary layer solution (green) with the scaled inner solution (red) near $z = 0$

According to the graph (2.11), it is appropriate to define the boundary layer thickness where 99% of the boundary values included. Therefore solving the linear part of the approximation with the 99% value,

$$1 - \frac{e^{\frac{2}{\sqrt{\varepsilon}}} + 1}{\sqrt{\varepsilon}(-1 + e^{\frac{2}{\sqrt{\varepsilon}}})} z_{boundary} \quad = \quad \frac{99}{100}. \tag{2.50}$$

We get the boundary layer solution as,

$$z_{boundary} \quad = \quad \frac{1}{100}\frac{\sqrt{\varepsilon}(-1+e^{\frac{2}{\sqrt{\varepsilon}}})}{e^{\frac{2}{\sqrt{\varepsilon}}}+1}. \tag{2.51}$$

As mentioned above there is another boundary layer near the z_* where $\alpha - \beta = 0$. There is a switch in stability from the equilibrium $P = 0$ to the non trivial equilibrium at this point. The following simplified model equation captures the behaviour near z_*.

$$\varepsilon\frac{\mathrm{d}^2P}{\mathrm{d}z^2} - (P - z\ H(z)) \quad = \quad 0, \tag{2.52}$$

where

$$P(-1) = 0 \text{ and } P(1) = 1. \tag{2.53}$$

Unlike my full Reaction Diffusion system this has an exact solution as a function of ε and this solution reads

$$P^*(z) \quad = \quad \frac{1}{2}\left(\frac{e^{\frac{z}{\sqrt{\varepsilon}}}\sqrt{\varepsilon}e^{\frac{1}{\sqrt{\varepsilon}}}}{e^{\frac{1}{\sqrt{\varepsilon}}}+e^{\frac{-1}{\sqrt{\varepsilon}}}} - \frac{e^{\frac{-z}{\sqrt{\varepsilon}}}\sqrt{\varepsilon}e^{\frac{-1}{\sqrt{\varepsilon}}}}{e^{\frac{1}{\sqrt{\varepsilon}}}+e^{\frac{-1}{\sqrt{\varepsilon}}}} - H(z)(-2z + e^{\frac{z}{\sqrt{\varepsilon}}}\sqrt{\varepsilon} - e^{\frac{-z}{\sqrt{\varepsilon}}}\sqrt{\varepsilon})\right). \tag{2.54}$$

As earlier, we subtract the outer solution $zH(z)$ from the exact solution (2.54). Then the inner solution reads,

$$P^*_{in}(z) \quad = \quad -\frac{1}{2}\left(\frac{\sqrt{\varepsilon}e^{\frac{1}{\sqrt{\varepsilon}}}(-e^{\frac{z+1}{\sqrt{\varepsilon}}} + e^{-\frac{z+1}{\sqrt{\varepsilon}}} + H(z)e^{\frac{z+1}{\sqrt{\varepsilon}}} + H(z)e^{\frac{z-1}{\sqrt{\varepsilon}}} - H(z)e^{-\frac{z-1}{\sqrt{\varepsilon}}} - H(z)e^{-\frac{z+1}{\sqrt{\varepsilon}}})}{e^{\frac{2}{\sqrt{\varepsilon}}}+1}\right) \tag{2.55}$$

As previously done, the inner solution was scaled so that its maximum is one, and this yields

$$P^*_{scaled}(z) \quad = \quad -\frac{e^{\frac{1}{\sqrt{\varepsilon}}}(-e^{\frac{z+1}{\sqrt{\varepsilon}}} + e^{-\frac{z+1}{\sqrt{\varepsilon}}} + H(z)e^{\frac{z+1}{\sqrt{\varepsilon}}} + H(z)e^{\frac{z-1}{\sqrt{\varepsilon}}} - H(z)e^{-\frac{z-1}{\sqrt{\varepsilon}}} - H(z)e^{-\frac{z+1}{\sqrt{\varepsilon}}})}{e^{\frac{2}{\sqrt{\varepsilon}}}-1} \tag{2.56}$$

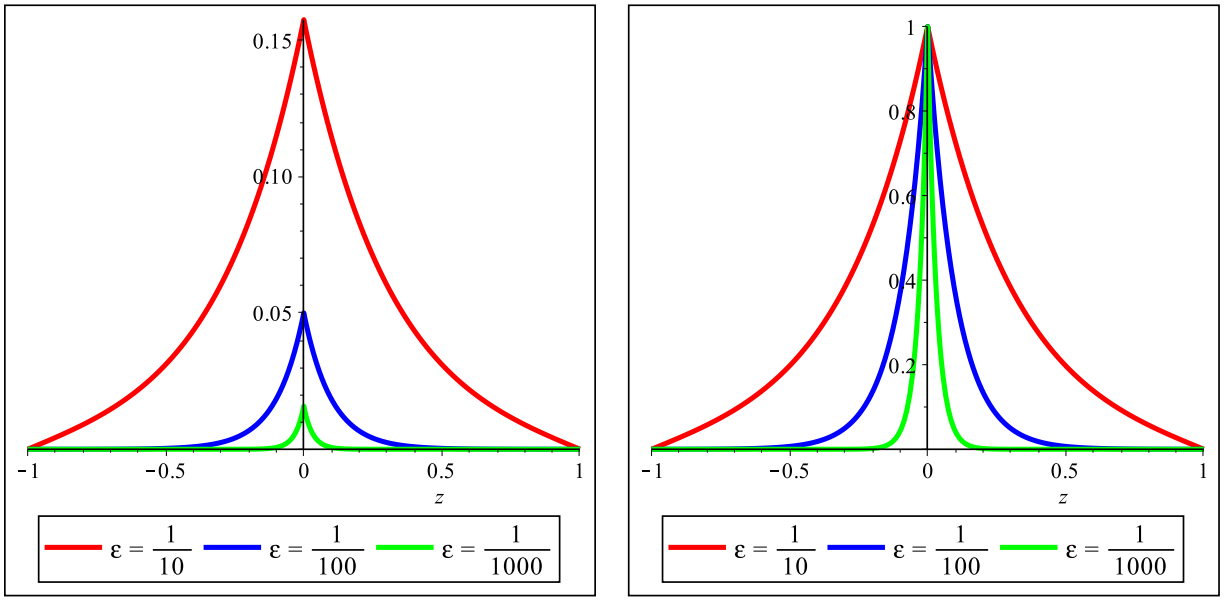

Figure 2.12: Left side graph represent the boundary layer near $z = z^*$ (2.55)for three different ε's. Right side graph represents the scaled boundary layer to its maximum (2.56).

It is important to notice that the inner solution at z^* has two parts, one for $z < 0$ and the other one for $z > 0$. According to the right side graph of figure (2.12) the inner solution is symmetric about $z = 0$, with a cusp at $z = 0$. Therefore the solution cannot be expanded as a series about $z = 0$. However, since we only care about the thickness of the boundary layer, we can select a 'one sided solution', and expand it to as a series, and only apply this series for the portion of the solution in which the series is valid. We choose the solution for $z < 0$, since this makes Heaviside function to zero, and hence simplifies the expression,

$$P^*_{scaled\ one\ sided}(z) \quad = \quad \frac{e^{\frac{1}{\sqrt{\varepsilon}}}(e^{-\frac{z+1}{\sqrt{\varepsilon}}} - e^{\frac{z+1}{\sqrt{\varepsilon}}})}{1 - e^{\frac{2}{\sqrt{\varepsilon}}}}. \tag{2.57}$$

Figure (2.13) shows the one sided solution with the scaled inner solution for $\varepsilon = \frac{1}{100}$. The linear approximation to the one sided scaled inner solution is,

$$P^*_{scaled\ one\ sided}(z) \quad = \quad 1 + \frac{e^{\frac{2}{\sqrt{\varepsilon}}} + 1}{\sqrt{\varepsilon}(-1 + e^{\frac{2}{\sqrt{\varepsilon}}})} z + O(z^2). \tag{2.58}$$

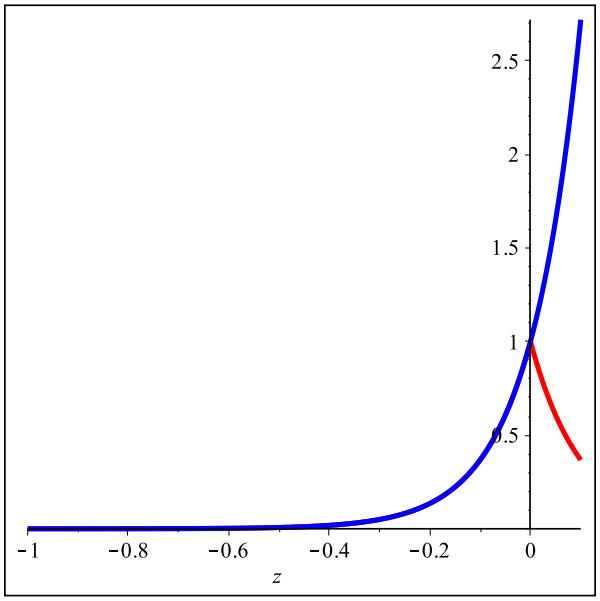

Figure 2.13: The boundary layer 'one sided' solution for $z < 0$ (blue) and scaled boundary layer solution (red) with $\varepsilon = \frac{1}{100}$

Then proceed with the same calculation as for the previous boundary layer.

$$1 + \frac{e^{\frac{2}{\sqrt{\varepsilon}}} + 1}{\sqrt{\varepsilon}(-1 + e^{\frac{2}{\sqrt{\varepsilon}}})} z \quad = \quad \frac{99}{100}. \tag{2.59}$$

Then we get the boundary layer thickness at z^* as,

$$z^*_{boundary} \quad = \quad -\frac{1}{100}\sqrt{\varepsilon}\frac{e^{\frac{2}{\sqrt{\varepsilon}}} - 1}{(1 + e^{\frac{2}{\sqrt{\varepsilon}}})}. \tag{2.60}$$

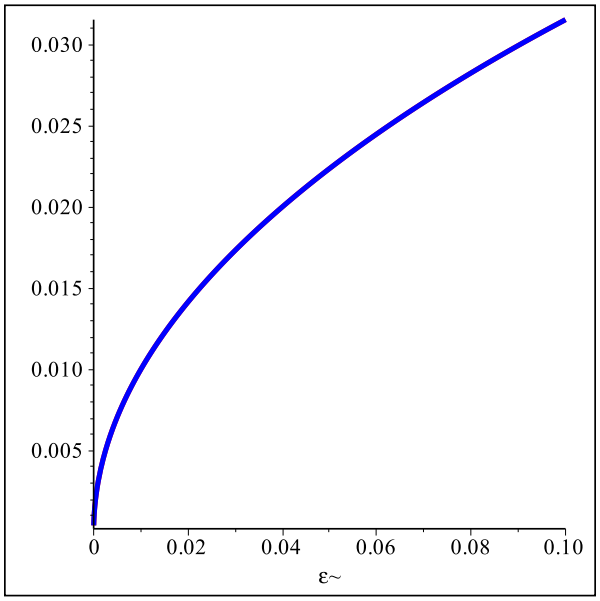

Figure 2.14: Boundary layer thickness at $z = 0$ (red) and (-)boundary layer thickness at $z = z^*$ (blue)

Figure (2.14) shows that in fact the thickness of the boundary layer is the same to first order, and scales roughly like the square root of the diffusivity. Estimating the scaling for the diffusivity allows us to qualitatively understand the essential features of the numerical solution.

In summary the above work allows us to reproduce the essential features of the preceding numerical simulations in augmented systems that have exact solutions which may be analyzed after the fact. Future work should aim to reconcile the reduced systems with the original system, perhaps with a detailed matched asymptotic analysis.

Chapter 3

A simple ecosystem model

3.1 What is an NPZD model

There are many difficulties in representing the complex biology of the marine ecosystem in terms of tractable mathematics. We follow the basic modelling approach of tracking "energy" as it moves between abstract modules of the model which correspond to different biological entities (e.g. zooplankton, phytoplankton, nutrients, etc.). Aside from the practical issues of data acquisition from observations and/or experiments, the primary issue is in deciding the number of modules that should be contained in the model [20]. Often this depends on the purpose of the experiment or fieldwork, though in the present case we are looking to explore theoretically more complex models than those of the previous chapter. Our model is based on four important components namely Nutrient, Phytoplankton, Zooplankton and Detritus (NPZD).

NPZD is a commonly used type of an ecosystem model [20]. The main idea of this chapter is to investigate the interactions of these variables based on the study of Soetaert and Herman [20]. The simulation carried out in Soetaert and Herman's study is written using R ,and in this chapter we develop the model in Matlab, supplementing it with a diffusion component similarly to [11]. We subsequently perform several numerical experiments to address the effect of varying model parameters that represent a variety of physical and biological processes (turbulence level, water turbidity, efficiency of predation, etc.).

3.2 A description of our model

There are many physical and biological conditions which effect the behaviour of any one member of an ecosystem. The implemented NPZD model considers four categories of variables in the somewhat abstract classes Nutrient, Phytoplankton, Zooplankton and Detritus. According to Soetaert [20] nitrate and ammonium are taken as the nutrient sources to the model and plants in the lake ecosystem as phytoplankton. Animals who graze upon phytoplankton are referred to as zooplankton. Detritus includes waste of zooplankton and phytoplankton by death or faeces. The model consists of 4 state variables that are connected with 7 flow rates.

The model thus solves four differential equations for the state variables. Spatial effects are included through a diffusion term which can be thought of as a very primitive parametrization of fluid turbulence. The diffusion terms are implemented using an implicit backward time stepping scheme on a Chebyshev grid in depth. The numerical method used here is the same method that is discussed in chapter 2.

The results are subsequently expressed graphically using MATLAB. We next discuss the basic formulation of the model, or in other words the flow chart, the conceptual model and its mathematical formulation. This is followed by a discussion of the design of the numerical experiments and a discussion of the individual experiments themselves.

3.2.1 Flow chart

This is the starting point of population modeling [20]. First we need to define the problem by identifying the main modules (state variables) represented by boxes, along with the flows which connect the variables, and describe the conversion of "energy" between them. Flows are represented by arrows connecting boxes. Figure (3.1) shows the flow chart of the model.

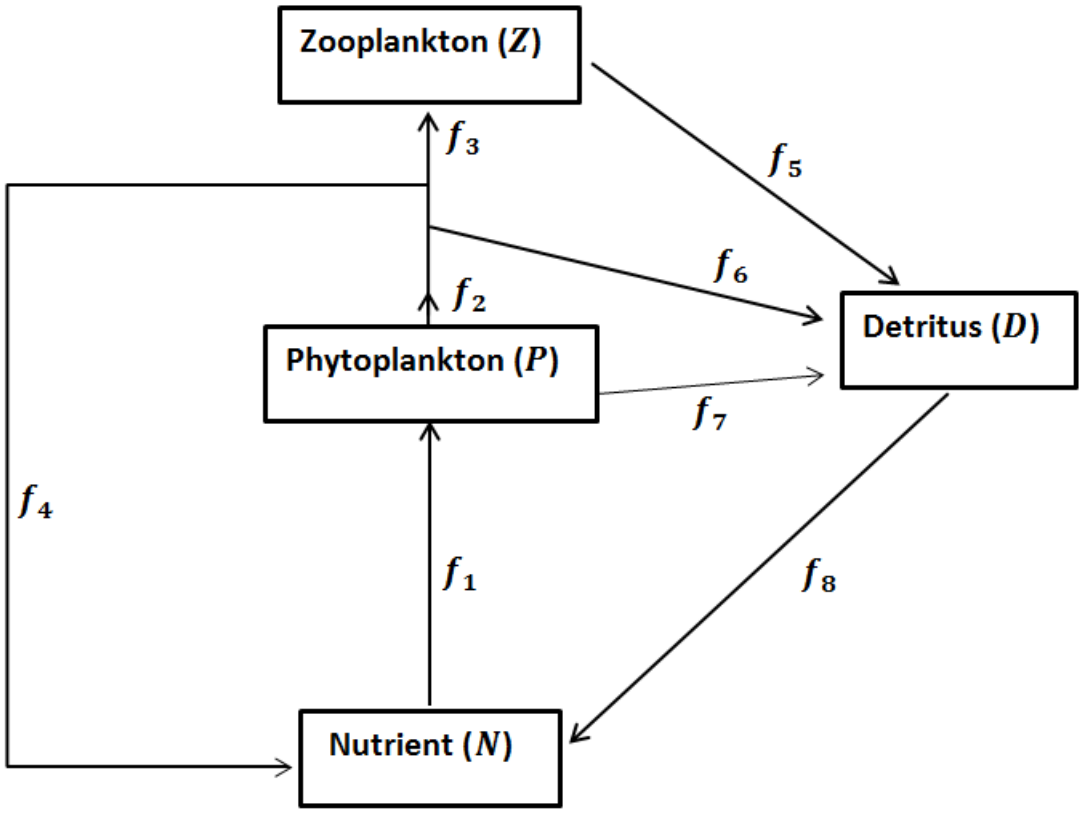

Figure 3.1: Flow chart for the Nutrients (N), Phytoplankton (P), Zooplankton (Z) and Detritus model.α and β are positive constants and I is the predation function.

f_1 = Nutrient uptake
f_2 = Zooplankton grazing
f_3 = Growth
f_4 = Nutrient excreation
f_5 = Death
f_6 = Nutrient uptake
f_7 = Phytoplankton loss (sinking)
f_8 = Detritus remineralisation

3.2.2 Conceptual model

The second step is the construction of a conceptual model which simplifies the system by using the flow chart, for each flow. This defines the time derivative of state variables, or in other words the rate of change of variables as a summation of sources and sinks. Arrow heads are drawn from the sinks and toward the sources. Below is the conceptual model for the NPZD model.

The differential equations for the changes of N,P,Z and D are given by,

$$\begin{aligned}
\frac{\mathrm{d}N}{\mathrm{d}t} &= \text{- Nutrient uptake + Detritus remineralisation + Nutrient excreation} \\
\frac{\mathrm{d}P}{\mathrm{d}t} &= \text{Nutrient uptake - Phytoplankton loss (sinking) - Zooplankton grazing} \\
\frac{\mathrm{d}Z}{\mathrm{d}t} &= \text{Growth - Death} \\
\frac{\mathrm{d}D}{\mathrm{d}t} &= \text{- Remineralisation + Zooplankton faecal + Zooplankton death + Phytoplankton loss}
\end{aligned} \tag{3.1}$$

Here time is measured in days and concentrations of N, P, Z, and D are measured in $mmolNm^{-3}$. All the parameters used are positive constants.

3.2.3 Mathematical formulation

In this step all the flows of the conceptual model are written as mathematical equations.

$$\begin{aligned}
\frac{\mathrm{d}N}{\mathrm{d}t} &= -\frac{N}{K_N+N}\mu\exp(\frac{-x}{\text{optLen}})P + kD + (1-\alpha-\beta)IZ \\
\frac{\mathrm{d}P}{\mathrm{d}t} &= \frac{N}{K_N+N}\mu\exp(\frac{-x}{\text{optLen}})P - m_1P - IZ \\
\frac{\mathrm{d}Z}{\mathrm{d}t} &= \alpha IZ - m_2Z \\
\frac{\mathrm{d}D}{\mathrm{d}t} &= -kD + \beta IZ + m_2Z + m_1P \\
I &= \frac{P}{K_p+P}I_{max}.
\end{aligned} \tag{3.2}$$

Below is a brief description of the terms in the equation(3.2).

According to Soetaert and Herman [20] when modelling the interaction between two modules, the key step is to identify the module which carries out the work and controls the maximal strength of the interaction [20]. So the maximum interaction is written as

$$\begin{aligned} \text{max\_ Interaction} &\propto \text{Worker} \\ \text{max\_ Interaction} &= \text{max\_Rate} \times \text{Worker}. \end{aligned} \tag{3.3}$$

Since max_ Interaction has to be bounded this should include a rate limiting term. The rate limiting term is a term influenced by either limited sources or inhibitors [20]. So the the interaction can be written as

$$\text{max\_ Interaction} = \text{max\_Rate} \times \text{Worker} \times \text{Rate\_ Limitation} \times \text{Rate\_ Inhibition} \\ . \tag{3.4}$$

When it comes to Nutrient uptake, equation (3.4) becomes,

$$\text{Nutrient Uptake} = \text{max\_Rate} \times P \times \text{Rate\_ Limitation} \times \text{Rate\_ Inhibition}. \tag{3.5}$$

since phytoplankton is the component which carries out the work. Here the rate limiting term should be a function of Nutrient [20].

Nutrient uptake is modelled by using a Michaelis - Menton function [20] $\frac{N}{K_N+N}$ as the rate limiting term. K_N is known as the half saturation constant [20]. The inhibition term is written as an exponential term using the optical length for decay of phytoplankton growth with depth. The growth rate decreases exponentially with depth due to light limitation.

Phytoplankton feed zooplankton and the model uses a predation function $\frac{P}{k_p+P} I_{max}$ to represent the grazing, which is again a Michaelis - Menton function. A fraction $\alpha < 1$ of the grazing of zooplankton is used for the growth of zooplankton and another fraction $\beta < 1$ is converted to detritus module as zooplankton feces. In this model zooplankton can graze only upon phytoplankton, whereas in reality they can graze upon detritus as well [25]. The production of zooplankton, zooplankton faeces and zooplankton excretion is modelled as a function of grazing.

$$\text{Zooplankton\_ Growth} = \text{growthRate} \times \text{Grazing}. \tag{3.6}$$

$$\text{Faeces} = \text{faecesFraction} \times \text{Grazing}. \tag{3.7}$$

$$\text{Zooplankton\_ Excretion} = \text{excretionRate} \times \text{Grazing}. \tag{3.8}$$

Detritus accumulates due to the death of phytoplankton and zooplankton, as well as the production of fecal pellets by the zooplankton. For spatial models detritus is assumed to diffuse like the other three categories, but to also sink with a constant settling velocity, w_s [11].

The death of zooplankton and phytoplankton are represented as,

$$\text{Zooplankton\_ Death} = \text{deathRate} \times \text{Zooplankton}, \tag{3.9}$$

and

$$\text{Phytoplankton\_ Death} = \text{lossRate} \times \text{Phytoplankton}, \tag{3.10}$$

respectively.

Finally, detritus undergoes a process known as remineralization which converts detritus to nutrients that can be reutilized by the phytoplankton,

$$\text{Remineralization} = \text{remineralizationRate} \times \text{Detritus}. \tag{3.11}$$

3.2.4 Consistency check

After the mathematical form, and interpretation of the individual flow terms are understood, the next step is to assess the consistency of the units. As an example consider the nutrient uptake. As described above

$$\text{Nutrient Uptake} = \text{max\_Rate}\frac{N}{K_N + N}\mu \exp(\frac{-x}{\text{optLen}})P, \tag{3.12}$$

here time is denoted per day and phytoplankton concentration is in $mmolNm^{-3}$. So the equation (3.12) becomes

$$mmolNm^{-3}d^{-1} \quad = \quad d^{-1}\left[\frac{mmolNm^{-3}}{mmolNm^{-3}+mmolNm^{-3}}\right], \tag{3.13}$$

and is consistent in terms of units. The rate of change of total mass should be equal to zero since there are no external sources and sinks [20], and this provides a second consistency check. The total rate of change of mass can be expressed as follows,

$$\frac{\mathrm{d}(\mathrm{Total\_\ mass})}{\mathrm{d}t} \quad = \quad \frac{\mathrm{d}N}{\mathrm{d}t}+\frac{\mathrm{d}P}{\mathrm{d}t}+\frac{\mathrm{d}Z}{\mathrm{d}t}+\frac{\mathrm{d}D}{\mathrm{d}t}=0, \tag{3.14}$$

and this confirms that the model is consistent for this particular component. The consistency of the other components can be confirmed in a similar manner.

3.3 Results of the model

3.3.1 Design of the experiments

The numerical experiments carried out are summarized in Table 3.1.

Label	Process Studied	Parameter varied	Parameter values
A	Strength of Diffusion	κ	0.0005, 0.001, 0.01
B	Effect of zooplankton growth rate	α	0.3, 0.7, 0.9
C	Effect of zooplankton feces rate	β	0.1, 0.3, 0.9
D	Effect of settling velocity	w_s	0, 0.1, 0.2
E	Decay of phytoplankton growth due to light	optLen	3,5,7

Table 3.1: Numerical experiments

Even for relatively simple models like the NPZD model, it is not easy to understand the entire parameter range since varying all the parameters would produce an unmanageable amount of data. Instead, it is more useful to study the effect of changes in important parameters with respect to a control case. All the experiments stated above are simulated

using the numerical method we discussed in chapter 2. 200 grid points has been used with a time step of 0.05. By varying the number of grid points (a maximum of 1000 points was used for one simulation, but others were more typically tried with between 100 and 400 grid points) we believe that this is a sufficient number of grid points to resolve the relevant dynamics. The Neumann boundary condition is enforced at the surface for N, P, Z and D. For the bottom, a Dirichlet boundary condition is enforced for N, P, Z and a Robin boundary condition is enforced on detritus. The latter allows for settling of detritus out of the water column. Initial conditions for N, P, Z, D are generated randomly using the randn MATLAB function. The experiments thus demonstrate the evolution of the system towards an equilibrium, though it should be noted it is the dynamics, as opposed to the final state, of the system that is more interesting in our case.

The parameter values used for the control case are summarized in Table 3.2.

Parameter varied	Parameter values
κ	0.001
α	0.7
β	0.3
w_s	0.1
optLen	5

Table 3.2: Values of parameters for the control case

All other parameter values which remained constant throughout the experiments are summarized in Table 3.3.

Parameter	Parameter values and units
μ	2 day^{-1}
K_N	1 $mmol\ Nm^{-3}$
K_p	0.7 $mmol\ Nm^{-3}$
m_1	0.1 day^{-1}
m_2	0.1 day^{-1}
k	0.05 day^{-1}
I_{max}	1.5 day^{-1}

Table 3.3: Values of other constant parameters used in the model

For the various models several standard plot types are used to illustrate the results. LIne plots at a fixed time demonstrate the features of the populations at a fixed moment in

time. While other measures (local averages for example) could be used, we found the single time plots useful in demonstrating how the various components of the NPZD model vary in size, and the space scales on which the plankton populations, in particular, vary. Space time plots allow the reader to contrast the evolution of all four variables with both depth (increasing to the right) and time (increasing upward). Downward propagating waves are thus shown as streaks with a positive slope, while upward propagating waves are indicated by streaks with a negative slope.

3.3.2 Experiment A

This introduces the basic model behaviour for the control case as well as how the changes in diffusivity effect the various fields, especially the nutrient concentration. Here the growth rate (α) is greater than faeces fraction (β). Figure (3.2) depicts the results of the control model with given parameter values.

According to the figure (3.2), the amount of nutrient gradually increases with the depth and has a maximum at a depth of 14 m, then decreases gradually. Phytoplankton has regions of large and small population up to 15 m and has zero population underneath. Zooplankton also has oscillations in population but the amplitudes of individual fluctuations is less than that of phytoplankton. Detritus has a maximum of 1.8 near the depth of 8 m.

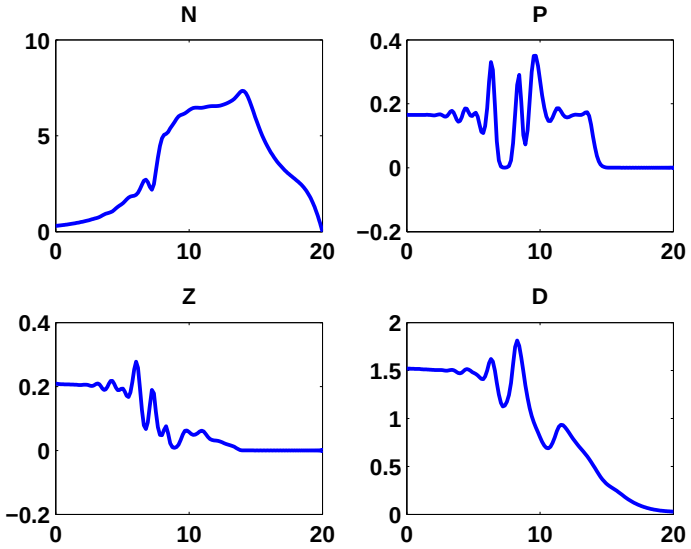

Figure 3.2: Solutions for the NPZD model (control case) at $t = 400$ days. Here $\alpha = 0.7, \beta = 0.3, \kappa = 10^{-3}, \text{optLen} = 5$

Figure (3.3) shows the nutrient concentration for different diffusion coefficients after 400 days. It clearly shows that increasing the diffusivity leads to a smoother nutrient concentration. It is also clear that there is a range of diffusivities for which qualitative features, like the fluctuations visible in the red and green curves appear.

Concentration of nutrient, phytoplankton, zooplankton and detritus after 400 days is represented in figure (3.4) for three different diffusivity values, κ. For all κ, phytoplankton and zooplankton concentration become zero below a depth of 15 m. This fact can be understood as follows. Production of phytoplankton is low near the bottom due to the absence of light which makes photosynthesis impossible. This in turn reduces the amount of zooplankton because of the lack of food. This also reduces the level of detritus as well, and according to the equation (3.2) detritus remineralizes to nutrient at a rate of k. On the other hand since the settling velocity for detritus is 10 cm per day, after 400 days a fecal pellet has traveled 40 m down. This can be another reason for why the concentration of detritus is nearly zero at and below 20 m. Note that diffusion is not strong enough to overcome the sinking.

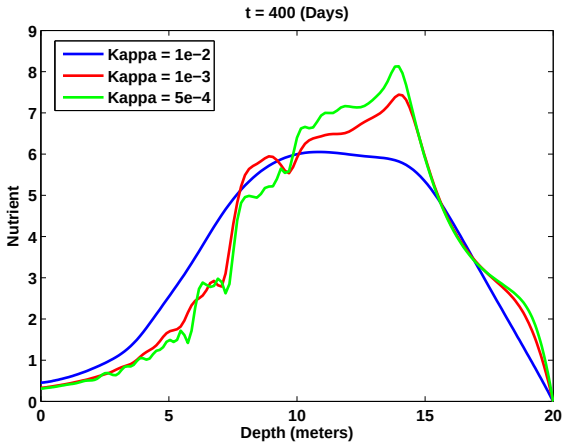

Figure 3.3: Nutrient concentration for different diffusion coefficients. $\alpha = 0.7, \beta = 0.3, \text{optLen} = 5, \text{settling velocity} = 0.1\text{m s}^{-1}$

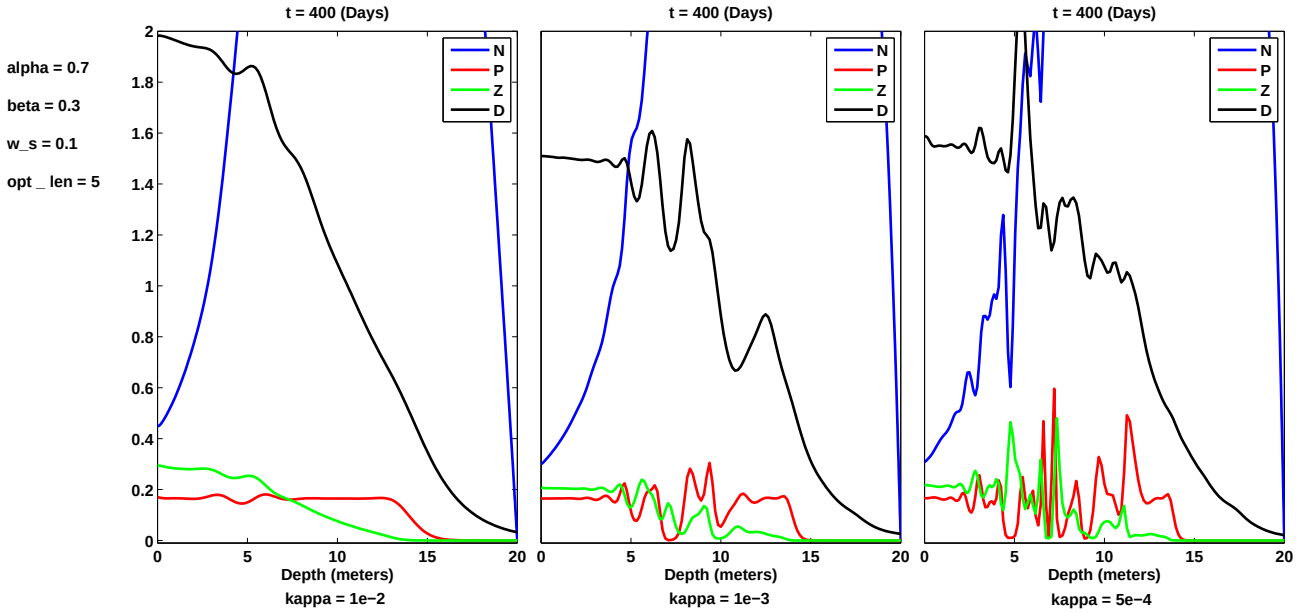

Figure 3.4: Solution for the NPZD model at $t = 400$ days for different values of κ. w_ s denotes the settling velocity. $\kappa = 10^{-3}$ represent the control case.

Figure(3.5) shows how the concentrations of N,P,Z and D for the control case, change with time and space while the figure (3.6) shows the concentrations for $\kappa = 5 \times 10^{-4}$.

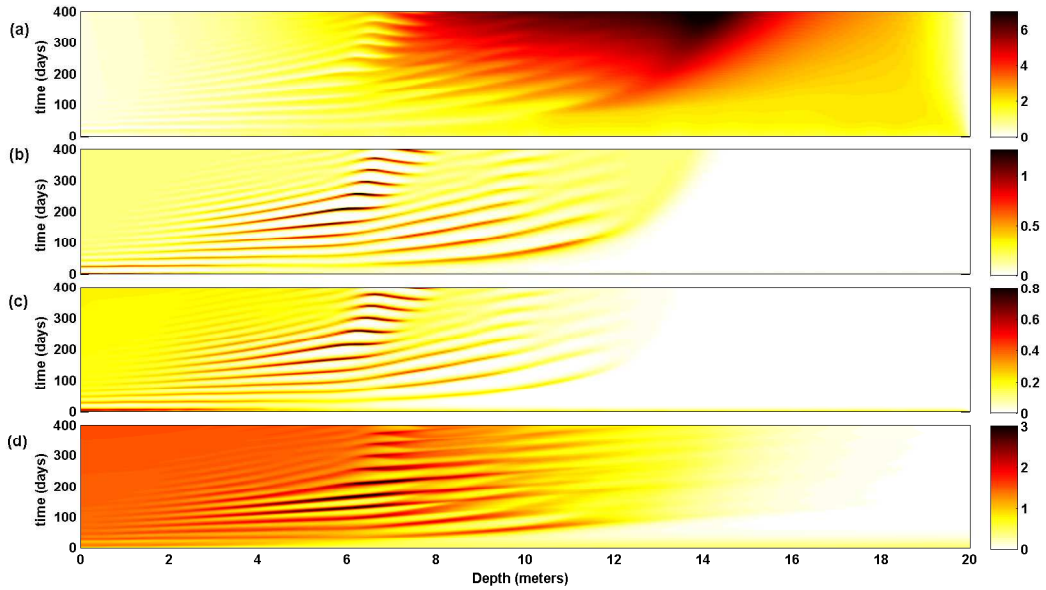

Figure 3.5: Space-time graph for the NPZD model (control case). (a) Nutrient (b) Phytoplankton (c) Zooplankton (d) Detritus at $t = 400$ days. $\alpha = 0.7, \beta = 0.3, \kappa = 10^{-3}$, optLen $= 5$, settling velocity $= 0.1$ m s^{-1}

The space-time plots in Figure (3.5) illustrate the qualitatively different behaviour of the four fields. The Nutrient, panel (a), is typically low in the near surface region, but increases to a peak value at depths between 8 and 14 meters. Before the high values are reached, streaks are visible. These represent travelling waves. They are more clearly visible in panels (b) and (c) which show the phytoplankton and zooplankton populations. It can be seen that there are periods of travelling waves (the streaks are not horizontal) and regions in which the population fluctuates in time only (the streaks are horizontal). From panel (d) it is clear that the detritus is maximal near the surface, though this is largely an artifact of the initialization. As the population evolves (the above discussed streaks in panels b and c) fluctuations in population are reflected in similar streaks in detritus concentration. For long times, detritus decays with depth, decaying to very low values below a depth of 14 meters or so (for the reasons discussed above).

These results can be compared and contrasted with a lower diffusivity case shown in Figure (3.6). A quick comparison suggests that many of the features remain quantitatively similar. However the fluctuations in plankton populations (panels b and c) are now more complex with some travelling waves for early times, followed by a complex pattern of spatio-temporal fluctuations after $t = 300$. Decreased diffusion increases the gaps in between

the streaks and this is more visible in plankton populations. This means that temporal fluctuations measured during this period would have a longer period.

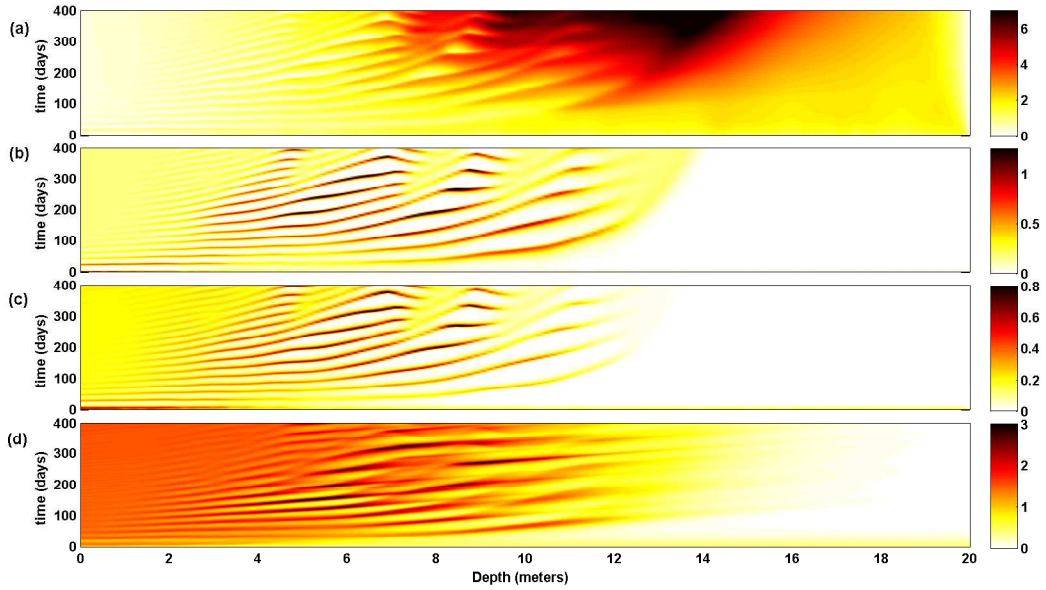

Figure 3.6: 2D graph for the NPZD model. (a) Nutrient (b) Phytoplankton (c) Zooplankton (d) Detritus at $t = 400$ days. $\alpha = 0.7, \beta = 0.3, \kappa = 5 \times 10^{-4}$, optLen $= 5$, settling velocity $= 0.1$ m s^{-1}

3.3.3 Experiment B

This experiment studies the behaviour of the model for different values of zooplankton growth rates. Figure (3.7) shows the behavior of N, P, Z and D with the change of zooplankton growth rate (α) where $\alpha = 0.7$ is the control case, after 400 days. The zooplankton growth rate is less (greater) than the control case on the left (right). It can be seen that when the growth rate is low, the rate of change of phytoplankton, zooplankton and detritus remain approximately zero above a depth of 10 m. In contrast, when zooplankton growth rate is higher than the control case ($\alpha = 0.9$) the graph shows small fluctuations in concentrations of phytoplankton, zooplankton and detritus near the surface as well as rapid change in between the depth of 5 m to 15 m.

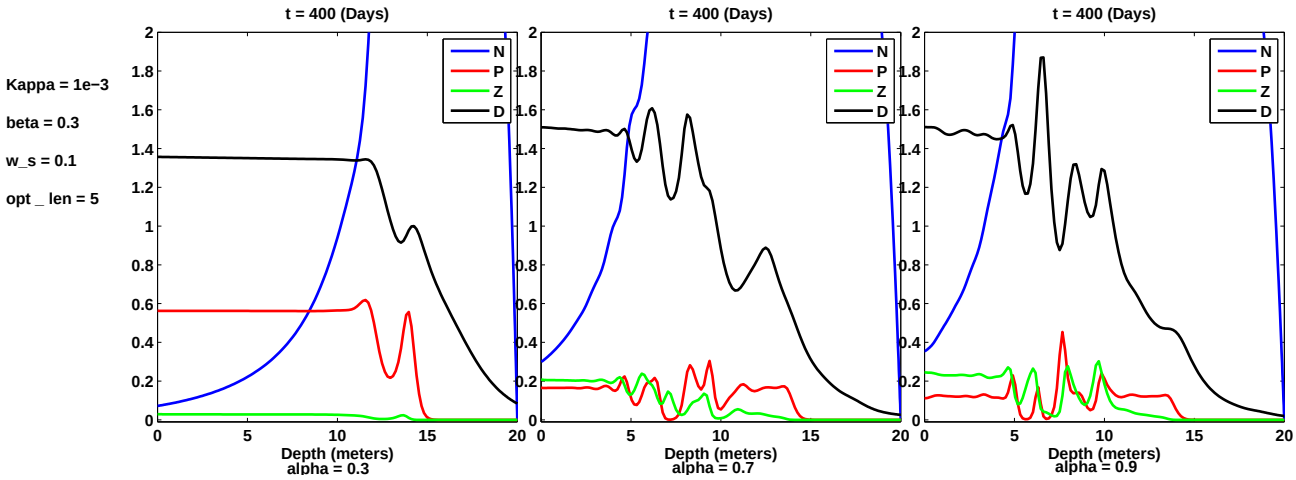

Figure 3.7: Solution for the NPZD model at $t = 400$ days for different values of α. w_ s denotes the settling velocity. $\alpha = 0.7$ represent the control case.

According to the equation (3.2), for smaller α, the rate of change of zooplankton concentration becomes smaller. This leads directly to an increase in the concentration of phytoplankton and reduces the detritus concentration, compared to the control case. In contrast, for lager α, zooplankton concentration increases and phytoplankton concentration decreases compared to the control case. Though, note that the fluctuations in phytoplankton population also increase.

Compared to the figure (3.5) for the control case, the figure (3.8) shows there are larger fluctuations in plankton concentration in between 5 m to 10 m after 200 days. For $\alpha = 0.9$ the concentration of nutrient and detritus (panels a and d) is more similar to the control case during all 400 days. This emphasizes the fact that even though zooplankton concentration is higher for $\alpha = 0.9$, detritus is affected much, and indeed detritus may be mostly increased by phytoplankton loss (death and sinking).

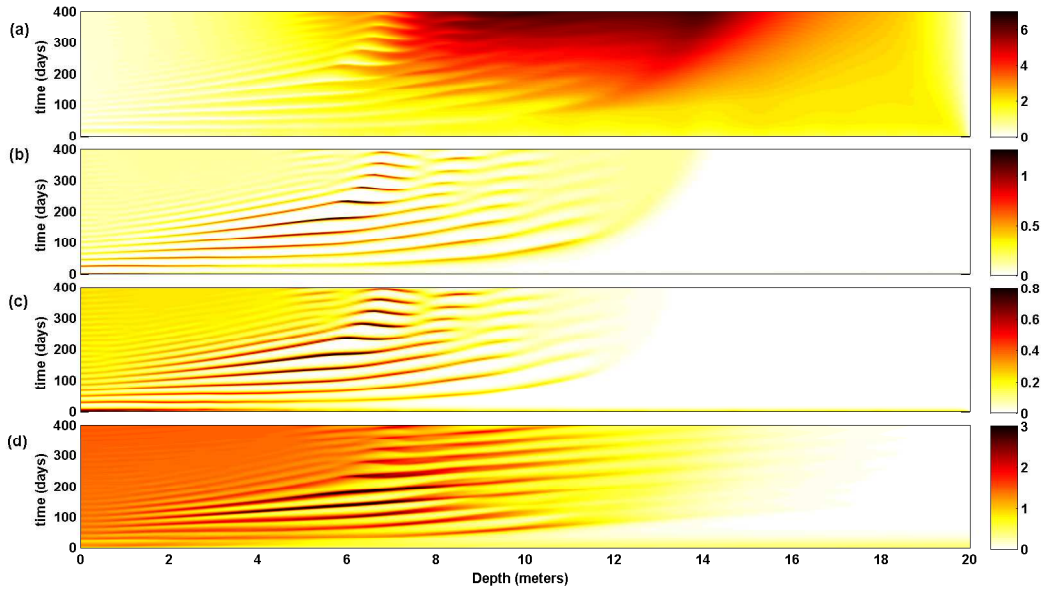

Figure 3.8: 2D graph for the NPZD model. (a) Nutrient (b) Phytoplankton (c) Zooplankton (d) Detritus at $t = 400$ days. $\alpha = 0.9, \beta = 0.3, \kappa = 10^{-3}$, optLen $= 5$, settling velocity $= 0.1$ m s^{-1}

3.3.4 Experiment C

This experiment was carried out to study the behaviour of model for different values of zooplankton faeces production rate. This ultimately varies the nutrient excretion rate. Figure(3.9) shows the behaviour of N, P, Z and D with the change of zooplankton faeces rate (β) and $\beta = 0.3$ is the control case. For smaller values of zooplankton faeces rate ($\beta = 0.1$) there is a quick increase of zooplankton concentration in between 5m - 10 m and at the same depth there is a quick drop of nutrient concentration.

According to the figure (3.9) for $\beta = 0.1$, zooplankton increment can happen due to increased phytoplankton grazing because of the the increased amount of nutrients uptake, since higher excretion. The drop of nutrient concentration can be explained by the factor of lesser demineralization due to lack of detritus. Again there is a quick drop of nutrients for larger values of zooplankton faeces rate ($\beta = 0.9$) and sudden peak of detritus in between 5 m -10 m. Compared to the control case, the concentration of detritus is high and the rate of change of nutrient is low. This is clear since larger β increases the amount of detritus and reduce nutrient excretion.

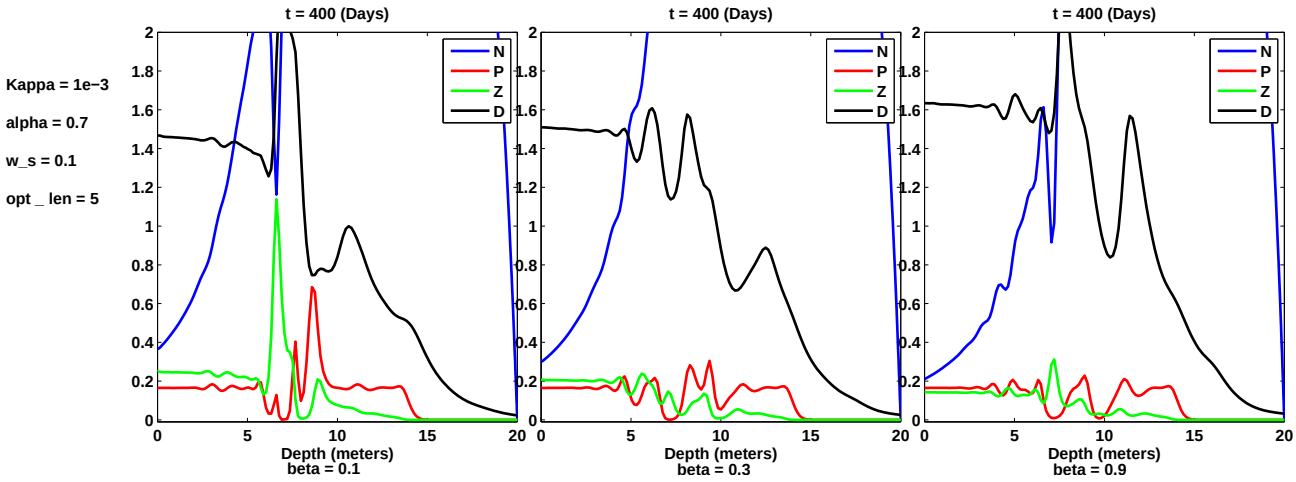

Figure 3.9: Solution for the NPZD model at $t = 400$ days for different values of β. w_ s denotes the settling velocity. $\beta = 0.3$ represent the control case.

Figure (3.10) clearly shows the increased number of travelling waves in the plankton population (panels b and c) for $\beta = 0.1$. The amount of detritus is low near the surface compared to the control case. There is a reduction in nutrient in between the depth of 8 m -14 m during the period from $200 - 300$ days. This is most likely due to the decreased remineralization.

Figure (3.11) clearly shows the zooplankon loss near the surface comparing to the control case and increased traveling wave activity in between $8m - 12$ m for both plankton types. Detritus is gained between 6 and 12 m , and is a direct result of more zooplankton death. There is a higher nutrient gain for $\beta = 0.9$ compared to the control case expressing the fact of higher remineralization.

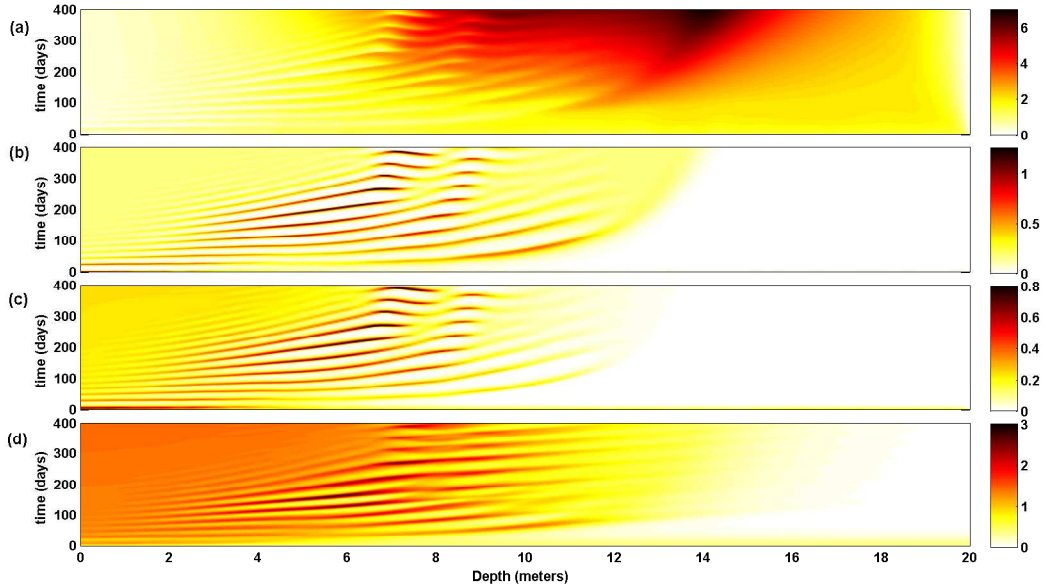

Figure 3.10: 2D graph for the NPZD model. (a) Nutrient (b) Phytoplankton (c) Zooplankton (d) Detritus at $t = 400$ days. $\alpha = 0.7, \beta = 0.1, \kappa = 10^{-3}, \text{optLen} = 5, \text{settling velocity} = 0.1 \text{ m s}^{-1}$

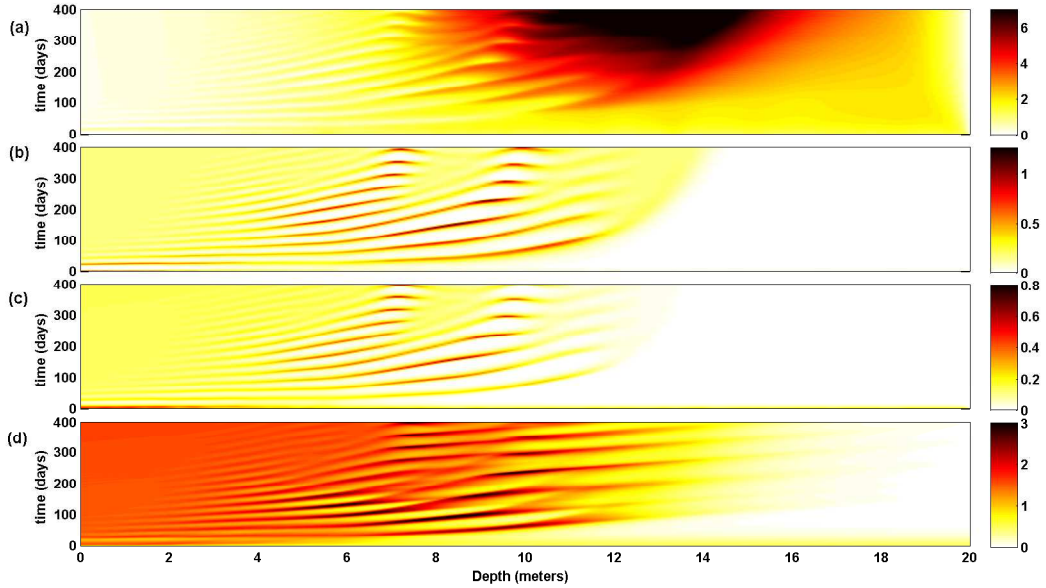

Figure 3.11: 2D graph for the NPZD model. (a) Nutrient (b) Phytoplankton (c) Zooplankton (d) Detritus at $t = 400$ days. $\alpha = 0.7, \beta = 0.9, \kappa = 10^{-3}, \text{optLen} = 5, \text{settling velocity} = 0.1 \text{ m s}^{-1}$

3.3.5 Experiment D

This experiment studies the fact of how the change of settling velocity changes the behaviour of the model. Settling velocity denotes the sinking velocity of detritus. For w_ s= 0, phytoplankton, zooplankton and detritus concentration become zero near the depth of 14 m according to the figure (3.12). Since there is no sinking of detritus in this case, detritus concentration drops faster than the control case with depth (there is nothing to either produce or transport detritus at depth). When w_ s= 0.2 m s $^{-1}$, which means the settling velocity for detritus is 20 cm per day (or after 400 days detritus can travel 80 m down) a rather unexpected result can be observed. Here the settling velocity of detritus is sufficient so that remineralization can take place at depth and hence there is a consistent downward flux of detritus from the top ten meters of the water column to the bottom ten meters of the water column so the detritus is not near to zero here at 20m.

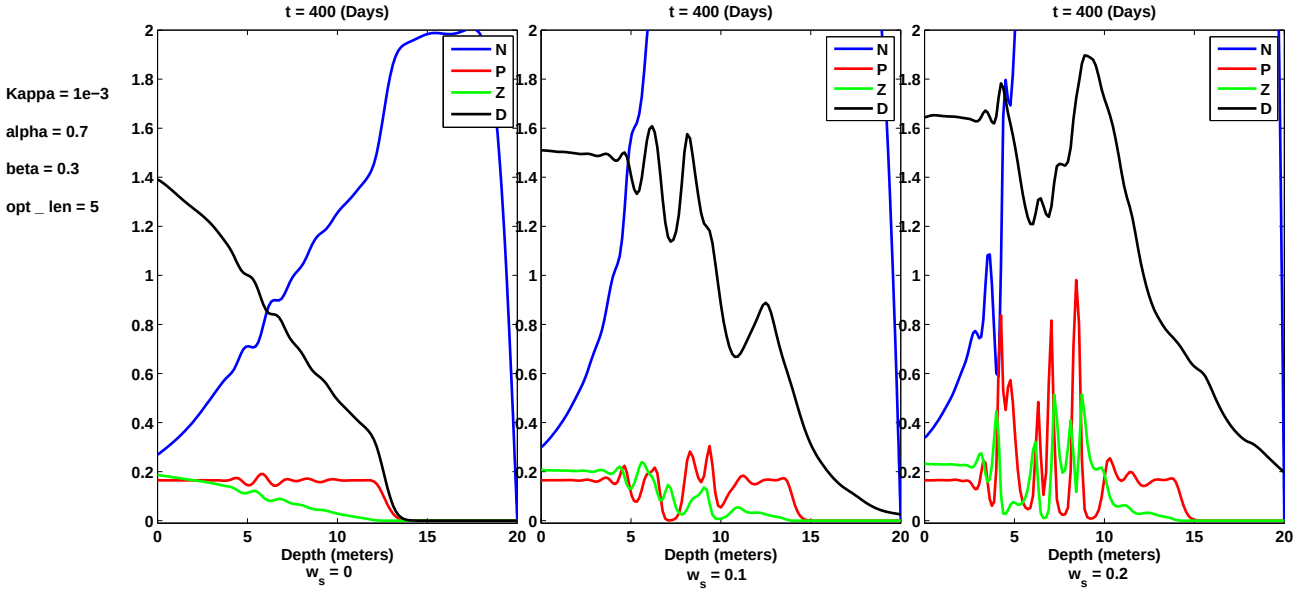

Figure 3.12: Solution for the NPZD model at t = 400 days for different values of w_ s, denotes the settling velocity. w_ s= 0.1 represent the control case.

Figure (3.13) shows a higher accumulation of detritus near the surface to a depth of 10 m since the detritus sinking velocity is zero. There is high nutrient concentration in between the depth of 10 m −20 m according to the figure (3.13). This is due to the lesser amount of nutrient uptake since there is a lack of phytoplankton and this in turn causes a reduction in the zooplankton concentration.

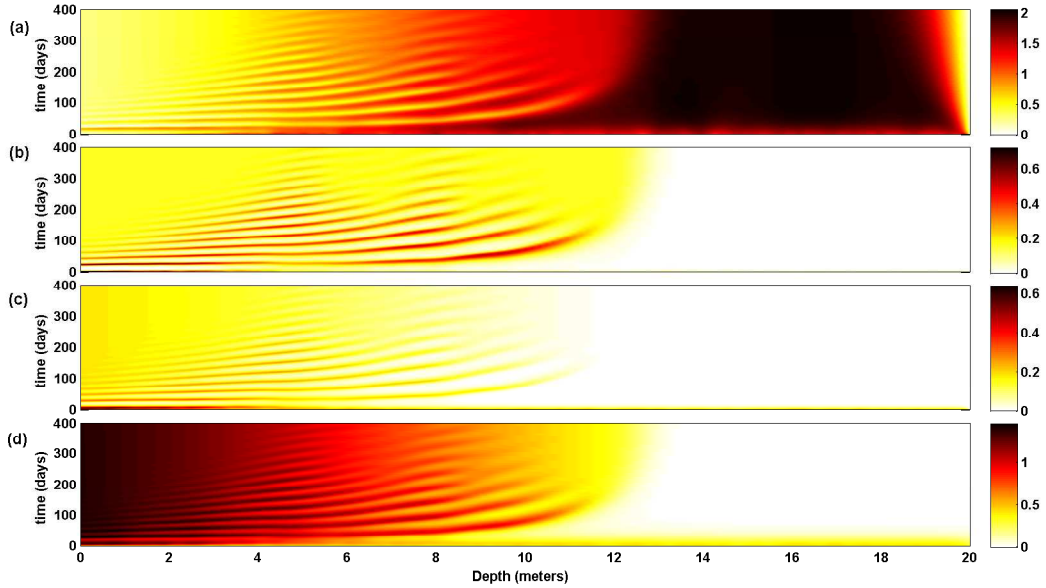

Figure 3.13: 2D graph for the NPZD model. (a) Nutrient (b) Phytoplankton (c) Zooplankton (d) Detritus at $t = 400$ days. $\alpha = 0.7, \beta = 0.3, \kappa = 10^{-3}$, optLen $= 5$, settling velocity $= 0$ m s^{-1}

Figure (3.13) shows a large amount of detritus from the surface to the depth of 10 m and no streaks with time compared to the control case figure (3.5). Plankton and detritus concentrations are both zero beneath a depth of 13 m during all 400 days.

3.3.6 Experiment E

This experiment is carried out to study the effect of optical length for decay of phytoplankton growth due to light limitation. According to the figure (3.15) when optLen is lower than the control case, the rate of change of nutrient is increased. This can be verified from the equation (3.2). The amount of detritus near the surface is high when optLen $= 3$.

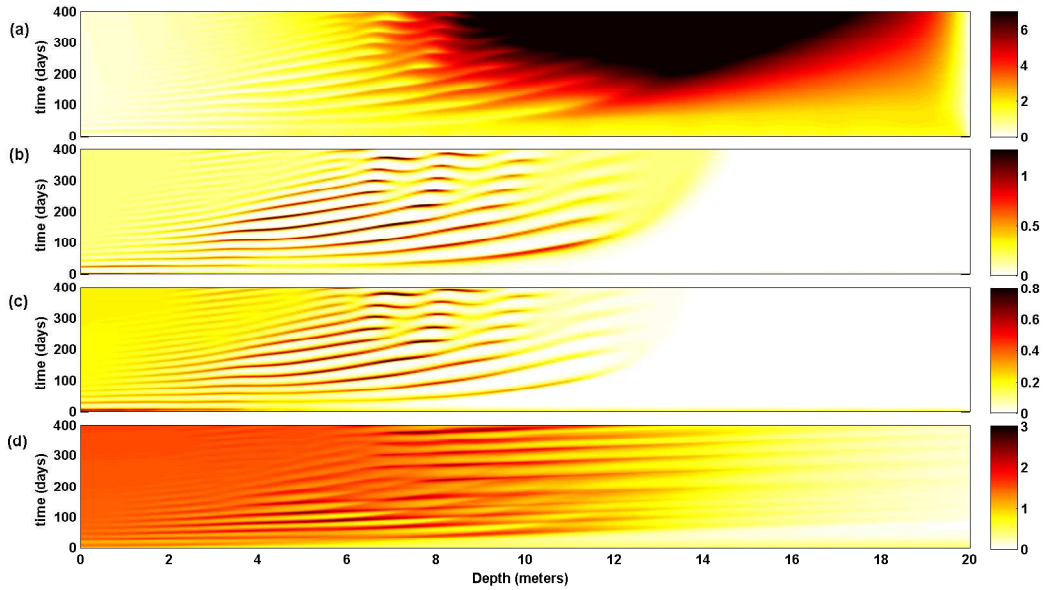

Figure 3.14: 2D graph for the NPZD model. (a) Nutrient (b) Phytoplankton (c) Zooplankton (d) Detritus at $t = 400$ days. $\alpha = 0.7, \beta = 0.3, \kappa = 10^{-3}$, optLen $= 5$, settling velocity $= 0.2$ m s^{-1}

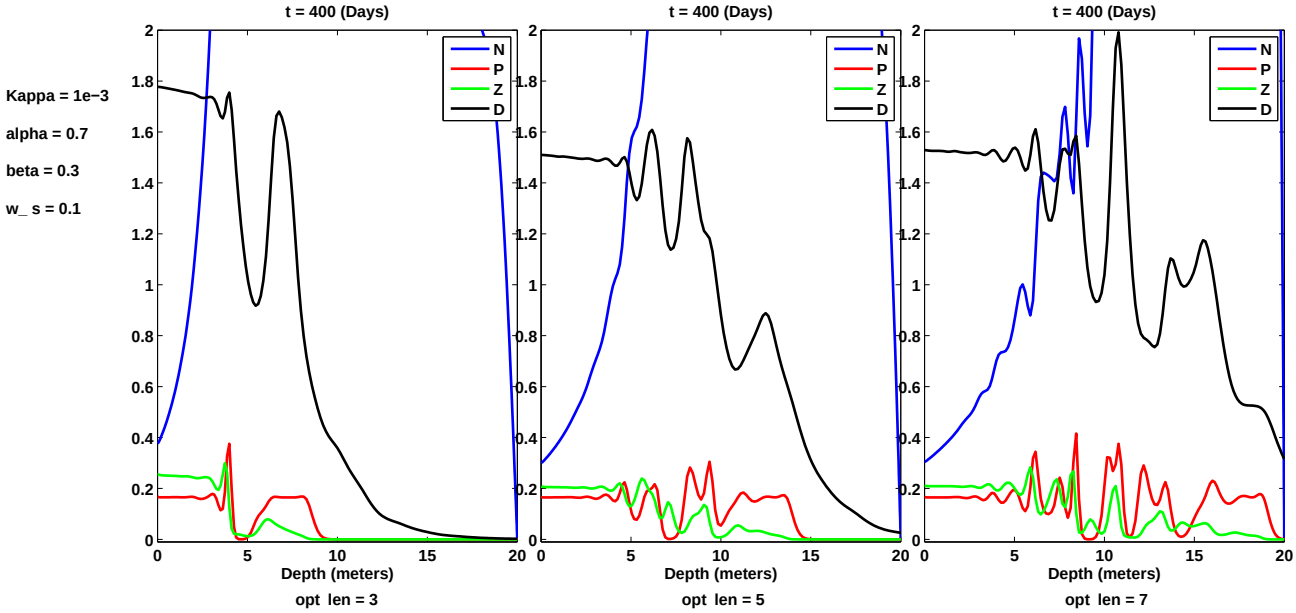

Figure 3.15: Solution for the NPZD model at $t = 400$ days for different values of optLen, denotes the optical length. optLen $= 5$ represent the control case.

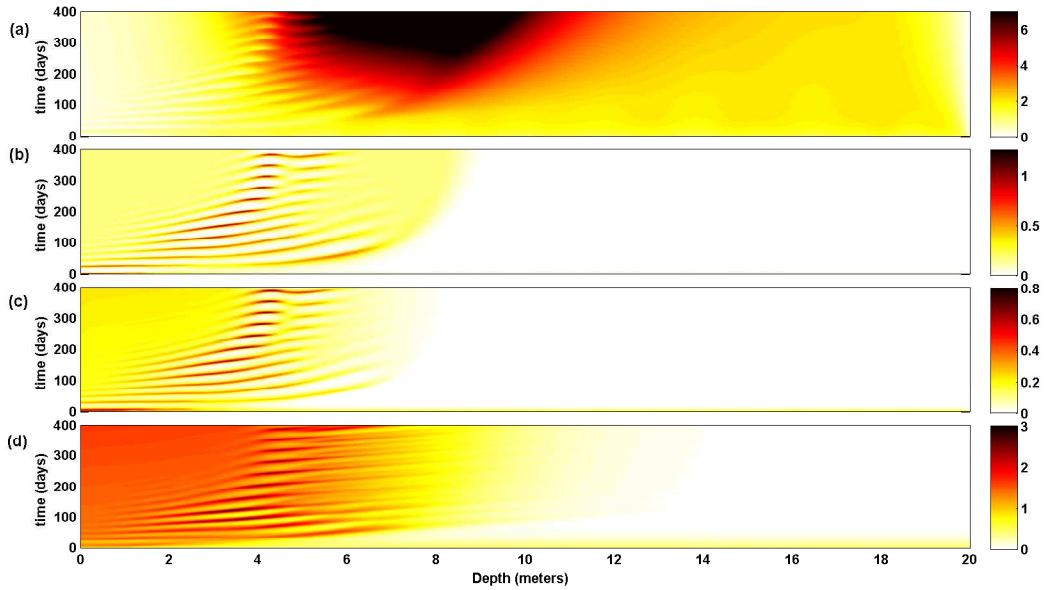

Figure 3.16: 2D graph for the NPZD model. (a) Nutrient (b) Phytoplankton (c) Zooplankton (d) Detritus at $t = 400$ days. $\alpha = 0.7, \beta = 0.3, \kappa = 10^{-3}$, optLen $= 3$, settling velocity $= 0.1$ m s^{-1}

Figure (3.17) shows that for higher values of optLen, higher nutrient concentration can be obtained closer to the bottom. Moreover, the dynamics of the plankton populations shifts to deeper water. This experiment thus highlights the important role of water clarity, for example turbid waters would be expected to have NPZD dynamics that are much more strongly trapped near the surface.

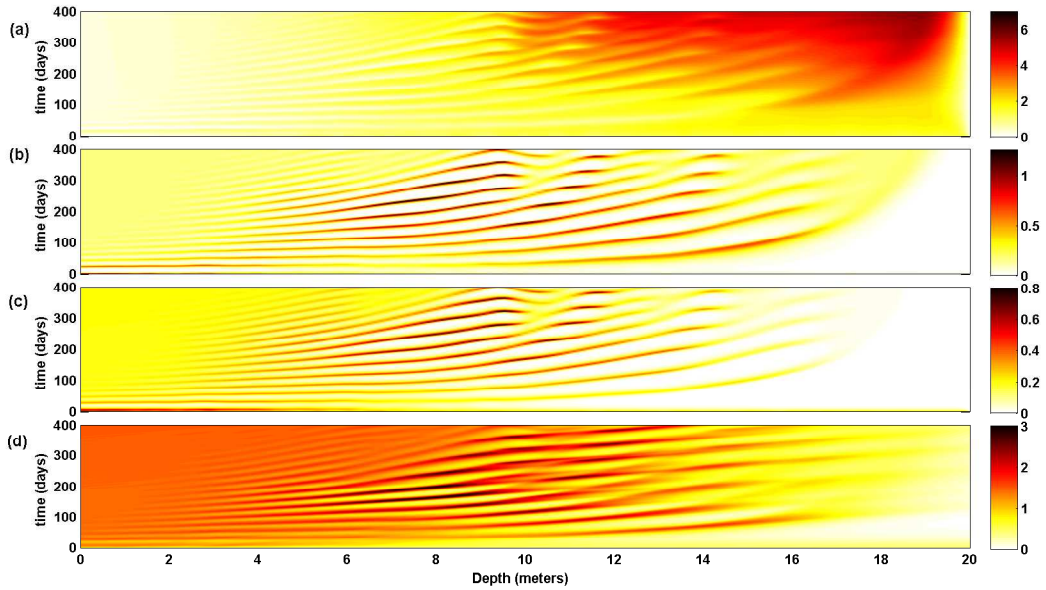

Figure 3.17: 2D graph for the NPZD model. (a) Nutrient (b) Phytoplankton (c) Zooplankton (d) Detritus at $t = 400$ days. $\alpha = 0.7, \beta = 0.3, \kappa = 10^{-3}$, optLen $= 7$, settling velocity $= 0.1$ m s^{-1}

3.4 Summary and Discussion

This chapter introduced a fairly simple NPZD model and conducted a variety of experiments to explore the model's parameter space. The intention of this section is to compare our model with a well known model from the literature, and to learn the basics of a well-studied type of model. Ice thus does not appear in this chapter.

In their paper, [11], Newberger and co-authors compare the behaviour of three types of ecosystem model: 1) NPZ (dissolved inorganic nitrogen, phytoplankton and zooplankton), 2) NPZD (dissolved inorganic nitrogen, phytoplankton, zooplankton and detritus), 3) NNPZD (Nitrate, Ammonium, phytoplankton, zooplankton and detritus) [11]. Apart from the terms discussed in the previous chapter, their model includes self shading by phytoplankton (higher populations block light from reaching populations below), and vertical and horizontal diffusion that may differ in magnitude. The model was also coupled to a simplistic ocean model [11] to study advection. The authors expended considerable effort in a search for periodic solutions. Given the very large number of parameters, the

authors expended a great deal of effort studying the behaviour their model under different physical and biological circumstances. The authors also studied the effect of light variation with depth, calculating the equilibrium points of the model and their stability for all three ecosystem model types. Newton's method was used in order to find the equilibrium solutions of the model.

Further Newberger *et al* coupled their model with a mixed layer model in order to include and describe many of the complex characteristics which were included in the Princeton Ocean Model (POM) by Spitz [11]. Newberger's coupled model is simple but includes a "standard" value for advection, a lesser value for horizontal diffusion and components varying with depth (concentrations) [11], in order to compare with previous results. The model parameters are chosen according to the oceanographic ecosystem [11] where their study is carried out, though the inherent uncertainty in the model parameters is not really characterized. The results of their models demonstrate the fact that both advection and horizontal diffusion are very important fact to figure out the plankton concentration [11]. The authors emphasize the fact that in order to get better results from ecosystem modeling, the correct form of zooplankton equation and suitable values for the parameters are essential. Their conclusion was that the mixed layer model with horizontal advection and sinking of both phytoplankton and detritus is a reasonable method for 2D ecosystem modeling.

The modelling carried out in this chapter, on the other hand, began with a modelling framework that builds a network which guarantees consistency. Once the model was shown to be mathematically valid, its behaviour was examined in five experiments that explore the parameter space. Even though there are millions of different experiments to do we chose this particular class of experiments, since we felt these vary the most crucial parameters independently (e.g the diffusion coefficient, growth rate, death rate, settling velocity and optical length). It was useful to understand the effect of parameter values towards the final result, though the details of the evolution were also shown to change (this was accomplished using space-time plots). Unlike [11] we did not focus on equilibrium solutions, choosing instead to evolve a random initial condition. This evolution was shown to be complex with both downward, and interestingly occasionally upward, propagating travelling waves in the plankton populations. While we did not couple our model with an ocean model (apart from the very simple diffusion parametrization of turbulence), the model is quite portable and could be couple to a simple ocean model in future work.

Chapter 4

Conclusion and Future Directions

In the previous chapters, we have shown both the complexity of the marine food web, and how mathematical modelling can be used to understand the dynamical behaviour of this ecosystem. While traditional modelling generally considers the open ocean, we have discussed simple models of ice algae. These organisms are differentiated from other planktonic organisms, by the fact that they live in a hostile and inaccessible environment. What is more this environment is rapidly changing under climate change. The physical conditions such as temperature, salinity, snow cover thickness, and light availability, all play a role in ecosystem models for ice algae. Due to the difficulty of formulating models of these processes, the literature on sea-ice ecosystem modelling is not older than three decades. The information and knowledge gathered is thus still quite limited.

This thesis has considered three main themes: 1) it reviewed the past sea-ice ecosystem studies, 2) it implemented simple ice-algae models, 3) it considered more complex plankton models of reaction diffusion type. The approach was somewhat different from the complex 2D model of Arrigo [30], which included three layers, ice growth rate, brine volume and salinity, grazing and excretion of algae, transport of nutrients in the SKL, and was thus more complex, and with many more parameters, than the models studied in this thesis. Our study considered a far simpler model, with a logistic growth term, which was subsequently improved with growth and death rates as exponentially decay functions with depth. In order to include the spatial spread of population, a diffusion term was introduced to the model. Then the reaction diffusion model equation was solved numerically using Strang splitting and Runge-Kutta methods for time discretization and the Chebyshev Pseudo Spectral method for spatial discretization. Even such a simple model was shown to exhibit two boundary layers. We developed a methodology to analyze and calculate the boundary layer thickness numerically as κ varies. From the results the scaling between the boundary

layer thickness and the diffusivity, κ, was calculated for the two boundary layers. Analogous problems were solved using asymptotic analysis for better understanding. While these results were interesting, they were likely an oversimplification of the ice algae ecosystem. To link the study with the plankton modelling literature, an NPZD model based on the study of Soetaert and Herman [20] was developed and discussed in detail. The model considered plankton growth and death, detritus remineralization, diffusive spreading of the various populations, as well as sinking of detritus. The model was examined using five different experiments, using the same numerical methods discussed above. These experiments tested the major types of variations in the model (such as water clarity, level of turbulence and so on). Taken together they suggest that certain aspects of the model are generic (such as propagating waves in the plankton populations) and others would be quite dependent on parameters that would need to be fitted from field measurements. Particularly interesting is the incidence of up propagating waves in the plankton population and it is these that form the key novelty of our simulations.

There are few other things to execute in oder to improve this model as a future study. The simple algae model currently includes growth and death rate as a function of only depth, but these could be implemented as functions of depth, temperature and salinity. More importantly, and following [11], the model could be coupled to a hydrodynamic model for various situations (for example tides or eddies). In the longer term, a more complete ice algae model should be developed, using the NPZD model as a template. In particular, it is very important to include a term which represents the flushing out of ice algae in brine channels that form during sea ice warming. Such a model could prove a useful component of future studies of climate change impacts on arctic ocean ecosystems.

References

[1] Protists. http://biology.unm.edu/ccouncil/Biology_203/Summaries/Protists.htm, accessed 05 August 2012.

[2] Daily pix. http://www.soleilorganique.com/sun-protection/seaweeds-place-in-the-sun/, accessed 08 July 2012.

[3] Giant algae blooms thriving under thinning arctic sea ice. http://www.cbc.ca/news/technology/story/2012/06/07/sci-phytoplankton-blooms-arctic.html, accessed 08 July 2012.

[4] Phaeophyta (brown algae). http://www.buzzle.com/articles/phaeophyta-brown-algae.html, accessed 08 July 2012.

[5] Algae and their characteristics, types of algae, ecological relationships, factors limiting the productivity of algae. http://science.jrank.org/pages/205/Algae.html, accessed 10 August 2012.

[6] Mathematical model. http://en.wikipedia.org/wiki/Mathematical_model, accessed 12 April 2013.

[7] Wikipedia. http://en.wikipedia.org/wiki/Algae, accessed 17 October 2012.

[8] Wikipedia. http://en.wikipedia.org/wiki/Crank-Nicolson_method, accessed 18 November 2012.

[9] Ecology global network. http://www.ecology.com/2011/09/12/important-organism/, accessed 20 September 2012.

[10] Magnificent marine algae blooms seen from space. http://www.wired.com/wiredscience/2010/08/phytoplankton-blooms-gallery/2/, accessed 20 September 2012.

[11] Newberger P. A., Allen J. S., and Spitz Y. H. Analysis and comparison of three ecosystem models. *Journal of Geophysical Research*, 108, 2003.

[12] Krembs C. and Deming J. Arctic theme page. *Sea ice: a refuge for life in polar seas?*, http://www.arctic.noaa.gov/essay_krembsdeming.html, accessed 10 August 2012.

[13] Lavoie D., Denman K., and Michel C. Modeling ice algal growth and decline in a seasonally ice-covered region of the arctic. *Journal of Geophysical Research*, 110, 2005.

[14] Press W. H., Teukolsky S. A., Vetterling W.T., and Flannery B. P. *Numerical Recipes in Fortran 77, Second Edition*. Press Syndicate of the University of Cambridge, Melbourne, Australia, 1992.

[15] Smith R. E. H., Anning J., Clement P., and Cota G. Marine ecology - progress series. *Abundance and production of ice algae in Resolute Passage, Canadian Arctic*, 48:251–263, 1988.

[16] Hawes I., Chresten L., Hansen L., Sorrell B. K., Nielsen M. H., Borzak R., and Buss I. Photobiology of sea ice algae during initial spring growth in kangerlussuaq, west greenland, insights from imaging variable chlorophyll fluorescence of ice cores. *Springer Science*, 112, 2012.

[17] LeVeque J. *Finite Difference Methods for Differential Equations, course notes for AMath 585-586*. University of Washington, 2005.

[18] Murray J.D. *Mathematical Biology I. An Introduction*. Springer, New York, 2001.

[19] Addy K. and Green L. Natural resources facts. *Algae in Aquatic Ecosystems*, 1996.

[20] Soetaert K. and Herman P. M. J. *A Practical Guide to Ecological Modelling*. Springer, Netherlands Institute of Ecology, 2009.

[21] Lamb K.G. *Course notes for AMath 732*. University of Waterloo, 2009.

[22] Pogson L., Tremblay B., Lavoie D., Michel C., and Vancoppenolle M. Development and validation of a one dimentional snow ice algae model against observations in resolute passage, canadian arctic archipelago. *Journal of Geophysical Research*, 116, 2011.

[23] Tedesco L., Vichi M., Haapala J., and Stipa T. A dynamic biologically active layer for numerical studies of the sea ice ecosystem. *Ocean Modelling*, 35, 2010.

[24] Bender C. M. and Orszag S. A. *Advanced Mathematical Methods for Scientists and Engineers*. McGraw Hill Book Company, New York, 1978.

[25] Edwards A. M. Adding detritus to a nutrient, phytoplankton, zooplankton model, a dynamical system approach. *Journal of Plankton Research*, 23, 2001.

[26] Jin M., Deal C. J., Wang J., Shin K. H., Tanaka N., Whitledge T. E., Lee S. H., and Gradinger R. R. Controls of the landfast ice ocean ecosystem offshore barrow, alaska. *Annals of Glaciology*, 44, 2006.

[27] Trefethen L. N. *Spectral Methods in MATLAB*. Philadelphia, 2000.

[28] Zhang Q., Gradinger R., and Spindler M. Boreal environment research. *Experimental study on the effect of salinity on growth rates of Arctic-sea-ice algae from the Greenland Sea*, ISSN 1239-6095, 1999.

[29] Arrigo K. R. Science. *Massive Phytoplankton Blooms Under Arctic Sea Ice*, 336, 2012.

[30] Arrigo K. R., Kremer J. N., and Sullivan C. W. A simulated antarctic fast ice ecosystems. *Journal of Geophysical Research*, 98, 1993.

[31] Durran D. R. *Numerical Methods for Fluid Dynamics with Applications to Geophysics*. Springer, USA.

[32] Nishi Y. and Tabeta S. Effects of atmospheric heat input on the release of organic carbon fromsea ice. *Journal of Marine Systems*, 67, 2006.